PALEOCEANOGRAPHY, VOL. 27, PA2207, doi:10.1029/2011PA002244, 2012

Rapid switches in subpolar North Atlantic hydrography and climate during the Last Interglacial (MIS 5e)

Nil Irvalı,[1,2] Ulysses S. Ninnemann,[1,2] Eirik V. Galaasen,[2] Yair Rosenthal,[3] Dick Kroon,[4] Delia W. Oppo,[5] Helga F. Kleiven,[1,2] Kate F. Darling,[4] and Catherine Kissel[6]

Received 8 October 2011; revised 27 March 2012; accepted 30 March 2012; published 12 May 2012.

[1] At the peak of the previous interglacial period, North Atlantic and subpolar climate shared many features in common with projections of our future climate, including warmer-than-present conditions and a diminished Greenland Ice Sheet (GIS). Here we portray changes in North Atlantic hydrography linked with Greenland climate during Marine Isotope Stage (MIS) 5e using (sub)centennially sampled records of planktonic foraminiferal isotopes and assemblage counts and ice-rafted debris counts, as well as modern analog technique and Mg/Ca-based paleothermometry. We use the core MD03-2664 recovered from a high accumulation rate site (~34 cm/kyr) on the Eirik sediment drift (57°26.34′N, 48°36.35′W). The results indicate that surface waters off southern Greenland were ~3–5°C warmer than today during early MIS 5e. These anomalously warm sea surface temperatures (SSTs) prevailed until the isotopic peak of MIS 5e when they were interrupted by a cooling event beginning at ~126 kyr BP. This interglacial cooling event is followed by a gradual warming with SSTs subsequently plateauing just below early MIS 5e values. A planktonic δ^{18}O minimum during the cooling event indicates that marked freshening of the surface waters accompanied the cooling. We suggest that switches in the subpolar gyre hydrography occurred during a warmer climate, involving regional changes in freshwater fluxes/balance and East Greenland Current influence in the study area. The nature of these hydrographic transitions suggests that they are most likely related to large-scale circulation dynamics, potentially amplified by GIS meltwater influences.

Citation: Irvalı, N., U. S. Ninnemann, E. V. Galaasen, Y. Rosenthal, D. Kroon, D. W. Oppo, H. F. Kleiven, K. F. Darling, and C. Kissel (2012), Rapid switches in subpolar North Atlantic hydrography and climate during the Last Interglacial (MIS 5e), *Paleoceanography*, *27*, PA2207, doi:10.1029/2011PA002244.

1. Introduction

[2] The climate of the last interglacial period, Marine Isotope Stage (MIS) 5e, has many features in common with model projections of our future climate. These include warmer-than-present climatic conditions, a significantly reduced Greenland Ice Sheet (GIS) and a higher sea level [e.g., *Otto-Bliesner et al.*, 2006; *Kopp et al.*, 2009]. Therefore, ocean-climate characterizations spanning the Termination II through the peak of MIS 5e (i.e., transition from a glacial state into a warmer-than-present climatic state) may provide important insights and constraints for better understanding the response of the ocean and the GIS to future warming and freshening. Such characterizations are essential in order to identify different interglacial climate and ocean circulation modes as well as any potential thresholds for switching between them. For example, several studies have now identified a climatic "pause" and/or a two-step deglaciation during Termination II, between MIS 6 and MIS 5e, from various regions in the North Atlantic [*Sarnthein and Tiedemann*, 1990; *Lototskaya and Ganssen*, 1999; *Sánchez Goñi et al.*, 1999; *Shackleton et al.*, 2002, 2003; *Gouzy et al.*, 2004; *Bauch and Erlenkeuser*, 2008]. Among these studies, *Shackleton et al.* [2002, 2003] provided a particularly detailed description of the penultimate deglaciation and the MIS 5e plateau in the subtropics using core MD95-2042 (Figure 1). During the early part of the benthic MIS 5e plateau following the MIS 6/5e transition, *Shackleton et al.*'s [2002] planktonic δ^{18}O record showed a

[1]Uni Bjerknes Centre, Uni Research, Bergen, Norway.
[2]Department of Earth Science and Bjerknes Centre for Climate Research, University of Bergen, Bergen, Norway.
[3]Institute of Marine and Coastal Sciences and Department of Geology, Rutgers, State University of New Jersey, New Brunswick, New Jersey, USA.
[4]School of GeoSciences, University of Edinburgh, Edinburgh, UK.
[5]Department of Geology and Geophysics, Woods Hole Oceanographic Institution, Woods Hole, Massachusetts, USA.
[6]Laboratoire des Sciences du Climat et de l'Environnement/IPSL, CEA/CNRS/UVSQ, Gif-sur-Yvette, France.

Corresponding author: N. Irvalı, Uni Bjerknes Centre, Uni Research, Allégaten 55, N-5007 Bergen, Norway. (nil.irvali@uni.no)

0883-8305/12/2011PA002244

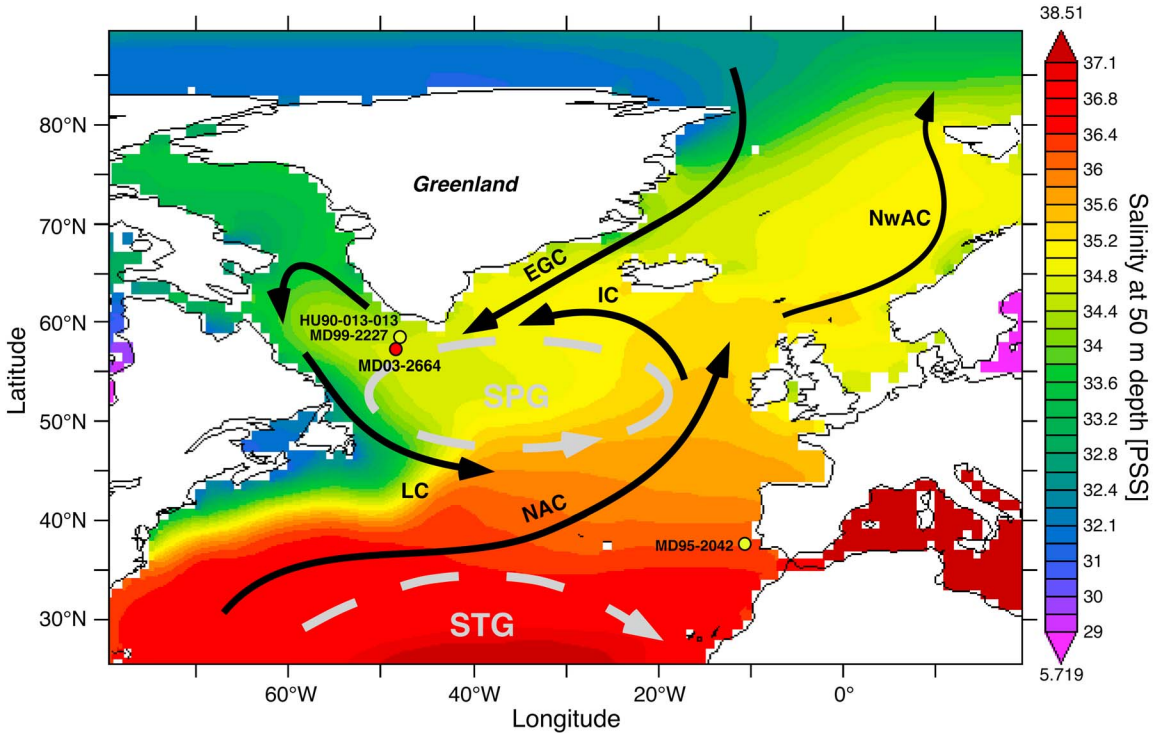

Figure 1. Map of the North Atlantic Ocean and the Nordic Seas. Arrows depict the schematic circulation and spreading pathways of the surface currents in the region. Colors indicate the Sea Surface Salinity (SSS) at 50 m depth (http://data.nodc.noaa.gov/las [*Antonov et al.*, 2010]). Location of core MD03-2664 (57°26.34′N, 48°36.35′W; 3440 m water depth) is marked with a red circle. Other cores discussed in the text (HU90-013-013 (58°12.59′N, 48°22.40W; 3380 m water depth) [*Hillaire-Marcel et al.*, 1994], MD99-2227 (58°12.46′N, 48°22.38′W; 3460 m water depth) [*Carlson et al.*, 2008], and MD95-2042 (37°48′N, 10°10′W; 3146 m water depth) [*Shackleton et al.*, 2000])) are marked with yellow circles (NAC: North Atlantic Current; NwAC: Norwegian Atlantic Current; IC: Irminger Current; EGC: East Greenland Current; LC: Labrador Current; SPG: Subpolar Gyre; STG: Subtropical Gyre).

clear and extended plateau marked by intermediary planktonic δ^{18}O values before reaching minimal 5e levels. Following this intermediate state, an abrupt shift toward low planktonic δ^{18}O values occurs at 126 kyr BP and persists for the remainder of MIS 5e [*Shackleton et al.*, 2002, 2003]. This abrupt planktonic δ^{18}O shift at 126 kyr BP is linked with the beginning of the Eemian Interglacial on land and characterized by a significant increase in Eurosiberian and Mediterranean vegetation on the Iberian Peninsula [*Sánchez Goñi et al.*, 1999; *Shackleton et al.*, 2003]. A similar early MIS 5e planktonic δ^{18}O plateau has recently been found in Nordic Sea records [*Bauch et al.*, 2011], raising the possibility that this 126 kyr BP transition marks a widespread shift between two different interglacial hydrographic states in the subtropical and subpolar regions.

[3] Here we investigate hydrographic variability in the NW subpolar gyre (SPG) in order to better characterize the spatial imprint of these hydrographic changes and understand the mechanisms underlying this sudden transition. Using new high-resolution multiproxy records from the Eirik Drift, a high accumulation rate site off southern Greenland, we reconstruct changes in the North Atlantic surface ocean hydrography and climate spanning the period from late MIS 6 through early MIS 5e.

2. Oceanographic Setting

[4] We use calypso Core MD03-2664 (57°26.34′N, 48°36.35′W; 3440 m water depth) that was cored during the IMAGES P.I.C.A.S.S.O cruise onboard R/V *Marion Dufresne* of the French Polar Institute (IPEV). MD03-2664 is located on the Eirik sediment Drift, off the southern tip of the Greenland margin, well situated to monitor changes in SPG hydrography (Figure 1). We investigate the SPG region because surface water hydrography in the northern North Atlantic is dominated by the dynamics of the SPG, which are linked in turn to both large scale surface climate variability (such as the North Atlantic Oscillation (NAO) [*Häkkinen et al.*, 2008]) and the North Atlantic thermohaline circulation (THC) [*Hátún et al.*, 2005, 2009]. The eastern, northward flowing segment of the gyre is dominated by the branches of the warm and saline waters of the North Atlantic Current (NAC), while the southward flowing, cold and fresh East Greenland Current (EGC) dominates the western part (Figure 1). The EGC is the major carrier of

cold freshwater and sea ice from the Arctic Ocean into the lower latitudes of the North Atlantic via the Fram Strait [*Aagaard and Carmack*, 1989]. In addition it transports the deep and intermediate waters exiting the Arctic Ocean and Atlantic Water re-circulating in the Fram Strait, which contributes to form the Denmark Strait overflow and North Atlantic Deep Water [*Rudels et al.*, 2002].

3. Materials and Methods

3.1. Sample Preparation

[5] The 5 m interval (2350–2850 cm) of the core spanning MIS 5e and its transitions was continuously sampled at 1-cm spacing. The samples were wet sieved at >63 μm. We used the >63 μm fraction for selection of foraminiferal specimens for stable isotope analysis, to study compositional changes in foraminiferal assemblages, count ice-rafted detritus (IRD), and perform Mg/Ca analysis on *N. pachyderma* (s).

3.2. Stable Isotopic Analyses

[6] Oxygen (δ^{18}O) and carbon isotope (δ^{13}C) analyses were performed on the planktonic foraminifera *Neogloboquadrina pachyderma* (sinistral) in order to reconstruct surface water physical properties. *N. pachyderma* (s) was picked from the 150–250 μm size fraction. Oxygen isotopes (δ^{18}O) were also analyzed on the benthic foraminifera *Cibicidoides wuellerstorfi*, picked from size fractions >150 μm and are used for isotope stratigraphy. The stable isotope analyses were measured on a Finnigan MAT 253 mass spectrometer at the stable isotope laboratory at the Department of Earth Science and Bjerknes Centre for Climate Research, University of Bergen. All planktonic samples were run in two replicates and benthic samples were run in two replicates when sufficiently abundant. Results are expressed as the average of the replicates and reported relative to Vienna Pee Dee Belemnite (VPDB), calibrated using NBS-19 – crosschecked with NBS-18. Long-term reproducibility (1σ) of in-house standards is equal to or better than 0.08‰ and 0.03‰ for δ^{18}O and δ^{13}C respectively, for samples between 10 and 100 μg.

3.3. Foraminiferal Assemblages

[7] Foraminiferal counts were performed every 8 cm throughout the core. The resolution was increased to every 4 cm on the 2570–2850 cm interval of the core, to provide detailed perspectives spanning the period from the MIS 6/5e transition through the isotopic peak of MIS 5e. Sediment samples of the size fraction >150 μm were split to give approximately 300 planktonic foraminifera for the counts in each sample. The actual number of planktonic foraminifera counted in a sample ranged from 261 to 936 specimens. The abundances of the most dominant species relative to the total planktonic foraminiferal assemblage were calculated. The coiling ratio of *N. pachyderma* (the percentage of right coiling (or left coiling) variety in total (right + left coiling varieties)) is also computed. Here we adopt the name *N. incompta* sensu for the right coiling *N. pachyderma* variety, as suggested by *Darling et al.* [2006].

3.4. Ice-Rafted Debris

[8] Lithic fragments (ice-rafted debris (IRD)) in the >150 μm fraction were counted to estimate the iceberg discharge. Counts were performed every 4 cm across the 2600–2850 cm interval of the core. At least 300 grains were counted in each sample. The results are expressed as the percentages of IRD grains relative to total entities (i.e., foraminifera) in each sample (IRD%).

3.5. Sea Surface Temperatures

[9] Sea surface temperatures (SSTs) were reconstructed using both Mg/Ca and faunal assemblages (Figure 2). Mg/Ca measurements were performed every 4 cm across the 2600–2850 cm core interval, on the planktonic foraminifera *N. pachyderma* (s), picked from the same samples used for stable isotopic and faunal analyses. *N. pachyderma* (s) is a polar species, found throughout the upper water column, abundantly in the upper 50–100 m, but also calcifies at depths between 100 and 200 m [*Bauch et al.*, 1997; *Simstich et al.*, 2003; *Jonkers et al.*, 2010]. *N. pachyderma* (s) blooms during the spring and in late summer [e.g., *Jonkers et al.*, 2010], and therefore the Mg/Ca analyses from *N. pachyderma* (s) would reflect spring or late summer SSTs. Samples consisting of ~40 individuals selected from the 150–250 μm fraction were gently crushed between two clean glass slides under a microscope to open the individual chambers, and transferred into acid-leached vials. The crushed foraminiferal tests were cleaned to remove various contaminating phases. The cleaning protocol used involved clay removal, followed by reductive and oxidative steps to remove metal oxides and organic matter respectively, weak acid leach and final dissolution in dilute HNO_3. Quality control during the cleaning steps is assured by using two blanks throughout all the cleaning processes. Measurements were carried out on a Finnigan MAT Element XR Sector Field Inductively Coupled Plasma Mass Spectrometer (ICP-MS), following the method outlined by *Rosenthal et al.* [1999], at the ICP-MS laboratory at the Institute of Marine and Coastal Sciences, Rutgers, The State University of New Jersey, USA. Contamination from adhered sediment was monitored using Fe/Ca and Al/Ca measurements (Figure 2c). Five out of 61 samples were rejected because of possible contamination.

[10] Core top calibrations assessing the Mg/Ca-temperature relationship in *N. pachyderma* (s) in the Norwegian and Arctic seas portray a complicated picture. In some, there is no correlation between Mg/Ca and the calcification temperature estimated from the oxygen isotopic composition of the tests or from assuming a designated calcification depth [e.g., *Meland et al.*, 2006; *Kozdon et al.*, 2009]. The apparent lack of temperature sensitivity is likely due to the difficulty of assigning accurate δ^{18}O values to the water profiles in this region (required for calculating isotopic temperatures), and the apparently variable calcification depth of this species [*Kozdon et al.*, 2009]. We convert our Mg/Ca data to temperature estimates using the linear core tops calibration of *Kozdon et al.* [2009] (Figures 2a and 2b), which is based on the correlation with calcification temperatures inferred from Ca isotopes between 3 and 6°C. The calibration breaks down below 3°C in the Arctic Sea and toward the Greenland margins. We note, however, that today our site is situated well within the tight calibration range. Furthermore, comparison with the *Nürnberg* [1995] data for the Norwegian Sea suggests that, within the analytical uncertainty associated with each method, this relationship may also be applicable to the wider temperature range of about 3 to 10°C, which covers our

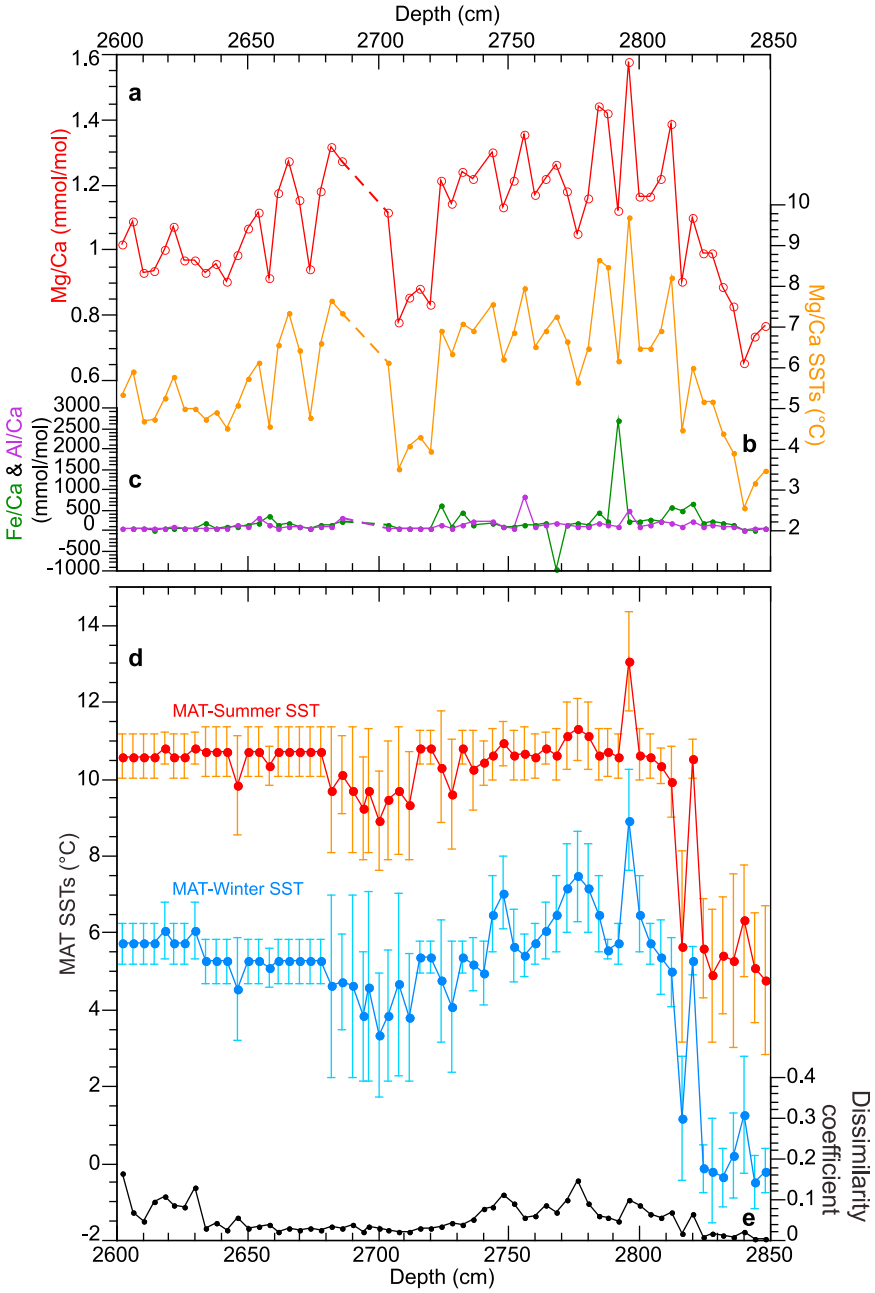

Figure 2. Sea surface temperature (SST) estimates from (top) Mg/Ca and (bottom) MAT plotted versus depth (cm): (a) Mg/Ca (mmol/mol) (red curve), (b) SST estimates from Mg/Ca (orange curve), (c) Fe/Ca (green curve) and Al/Ca (purple curve). The dashed lines represent an interval where 3 SST estimates were rejected due to possible contamination. (d) SST estimates from MAT. Error bars on the MAT estimates are the standard deviation of the estimates from top five analogs; (e) MAT dissimilarity coefficients.

reconstructed temperatures. Comparing the different data sets is not straightforward as each was obtained by using a different analytical method. For example, *Nürnberg et al.* [2000] suggested that his 1996 calibration data obtained by electron microprobe is about 5% higher than data obtained by ICP-OES on samples cleaned without any reductive step. In contrast with the calibration data, our down core data was obtained with the reductive step included in the cleaning protocol, thus a correction for the difference in cleaning methods is required. Previous studies demonstrate that adding the reductive step typically lowers the Mg/Ca results by 10–15% [*Rosenthal et al.*, 2004; *Meland et al.*, 2006]. To account for this difference we corrected the intercept in the original calibration of *Kozdon et al.* [2009] by −10% and use the following equation: Mg/Ca = 0.13T + 0.32. Considering all these uncertainties, the error on the combined calibration is about ±0.4°C (1 SEE) for temperatures >3°C. The long-term external precision of Mg/Ca analysis was ∼1.5% (1σ RSD) as determined by repeated measurements of a consistency standard with Mg/Ca ratio of 1.2 mmol/mol. The error in replicate samples is <0.1 mmol/mol. Thus we estimate the pooled error in individual temperature estimates to be about ±1.7°C

(2 SEE). We have further calculated the $\delta^{18}O$ in seawater ($\delta^{18}O_{sw}$), using Mg/Ca derived SSTs together with the paleotemperature equation of *Shackleton* [1974], with a VPDB to SMOW $\delta^{18}O$ conversion of 0.27‰. Applying this approach to core top Mg/Ca and $\delta^{18}O$ values of *N. pachyderma* (s) analyzed in a nearby multicore [*Kleiven et al.*, 2010] proxy SST and $\delta^{18}O_{sw}$ estimates reproduce modern oceanographic values—core top SST = 5.4 ± 1.1°C and $\delta^{18}O_{sw} = -0.03 \pm 0.29$‰ (2SEE n = 3) versus spring ocean temperature of 3.7°C [*Locarnini et al.*, 2010] and regional near surface $\delta^{18}O_{sw}$ values of approximately −0.2‰ ± 0.2 [*LeGrande and Schmidt*, 2006]. Sea Surface Salinity (SSS) estimates were derived from $\delta^{18}O_{sw}$ values, using a regional North Atlantic $\delta^{18}O_{sw}$-salinity relationship $\delta^{18}O_{sw} = (0.57 \pm 0.17)S-(19.8 \pm 5.9)$ [*LeGrande and Schmidt*, 2006]. The estimated standard error for absolute salinity reconstructions varies in different periods between ∼0.7 and 1.1 psu (2 SEE). This uncertainty combines the errors in temperature estimates (±1.7°C) and uncertainty in the choice of $\delta^{18}O_{sw}$-S relationship for this region. The latter takes into account modern changes in the local $\delta^{18}O_{sw}$-S relationship due to varying freshwater sources (e.g., ice sheet and sea ice changes). Nonetheless, larger variations in $\delta^{18}O_{sw}$ might have occurred either due to variation in global seawater during MIS 5e and larger glacial meltwater inputs. Due to the potentially large uncertainty in salinity estimates, we focus our discussion and comparison to modern water masses on $\delta^{18}O_{sw}$ changes—providing quantification for salinity that should be considered indicative.

[11] The Modern Analog Technique (MAT) estimates SSTs using a dissimilarity measure to match the foraminiferal assemblage of downcore samples with the assemblages found in worldwide modern core top database [*Hutson*, 1980; *Prell*, 1985]. In MAT SST estimates, the squared chord distance (SCD)—a signal to noise measure, is the most reliable equation for running MAT [*Overpeck et al.*, 1985]. In this study we generated SST estimates from planktonic foraminiferal assemblages using MAT [*Prell*, 1985] and the core top faunal and SST data from 527 Atlantic cores in the Brown University core top database [*Prell et al.*, 1999]. We used the SCD to determine the dissimilarity between the modern and fossil foraminiferal assemblages. Core tops that showed a dissimilarity greater than 0.4 were not considered when compiling the list of five analogs for the SST calculation. A high dissimilarity coefficient indicates there is a no-analog condition, where no modern analogs exist in the core top database. Although we have generated MAT SSTs on the same samples as the foraminiferal counts were performed, our main focus is the 2600–2850 cm interval, which spans the period from the MIS 6/5e transition through the isotopic peak of MIS 5e. At site MD03-2664, the average dissimilarity coefficient through the 2600–2850 cm interval is 0.053 with a standard deviation of 0.0139. The averages of summer and winter SST standard deviations are 0.9°C and 1.0°C respectively. High standard deviation of the SST estimates (≥2°C) during a small section of MIS 6 and MIS 5e indicate low confidence in the estimates for these samples (Figure 2d). Low dissimilarity coefficients (≤0.1) derived from the five best analogs suggest reliable SST estimates for most of MIS 6 and MIS 5e (Figure 2e).

3.6. Chronology and Sedimentation Rates

[12] *Shackleton et al.* [2002, 2003] developed a radiometrically constrained time scale for MIS 5 that is independent of astronomical calibration, using sediment core MD95-2042 (37°48′ N, 10°10′ W; 3146 m water depth), from the Iberian Margin. They defined the beginning of the MIS 5e plateau at 128 kyr BP, and termination of the plateau at 116.1 kyr BP, based on *Stirling et al.*'s [1998] age estimates for the MIS 5e sea level highstand. Here we apply the chronology of *Shackleton et al.* [2002, 2003], tuning the benthic $\delta^{18}O$ records of Core MD03-2664 to Core MD95-2042. We adopted tie points at 135 kyr BP, 128 kyr BP, 116.1 kyr BP and 113 kyr BP based on the benthic $\delta^{18}O$ records (Figure 3a). Note that temporal offsets (and associated uncertainties) of up to few thousand years are possible between benthic $\delta^{18}O$ records from different oceans, hemispheres, and water masses [e.g., *Skinner and Shackleton*, 2005; *Govin et al.*, 2012]. Here we tie records from two sites located within the same basin (i.e., North Atlantic), in similar water depths, that are both bathed by (proto) North Atlantic Deep Water. Based on this rationale, the sites should experience broadly similar benthic $\delta^{18}O$ influences/changes through time—minimizing the largest of the potential offsets associated with this approach. After adopting the benthic $\delta^{18}O$ derived age control points we compared the planktonic $\delta^{18}O$ record of Core MD95-2042 with the planktonic $\delta^{18}O$ record of Core MD03-2664 (Figure 3b). The sharp transition toward low planktonic $\delta^{18}O$ in MD03-2664 is approximately coeval (<500 years offset) with the abrupt planktonic $\delta^{18}O$ shift at 126 kyr BP described by *Shackleton et al.* [2003] in Core MD95-2042. While, as noted above, the stratigraphic constraints provided by benthic $\delta^{18}O$ are not precise enough to confirm that these are coeval events, the similarity in both character and timing between these two planktonic $\delta^{18}O$ records is compelling (Figure 3b). For the purposes of this paper we assume that the sharp planktonic $\delta^{18}O$ decrease in both records is a common event and adopt an additional age control point at 126 kyr BP. We note that while this assumption has little effect on the absolute age, it is relevant to our later discussion of these events as a common feature. The resulting age model at site MD03-2664 gives mean sedimentation rates of ∼34 cm/kyr for the MIS 5e plateau (128–116.1 kyr BP), corresponding to a mean temporal sample spacing of ∼29 years/cm (Figure 3c).

[13] Sedimentation on the Eirik Drift is strongly affected by the strength and position of the Western Boundary Undercurrent (WBUC). Glacial-interglacial changes in the depth and/or vigor of the WBUC, which supplies sediments to the Eirik Drift, results in expanded interglacial and condensed glacial sediment sequences in the deep parts of the Eirik Drift sediment cores [e.g., *Hillaire-Marcel et al.*, 1994, 2001; *Hunter et al.*, 2007]. Previous work in the region has shown evidence for variable rates of sediment input in the region due to detrital layer input associated with ice sheet instabilities [e.g., *Evans et al.*, 2007], detritus shedding from Greenland margin, spillover from distal Northwest Atlantic Mid-Ocean Channel (NAMOC) turbidites, or velocity fluctuations in the contour currents supplying sediments [*Hesse and Chough*, 1980; *Chough et al.*, 1987; *Hiscott et al.*, 1989]. High interglacial sedimentation rates can also be

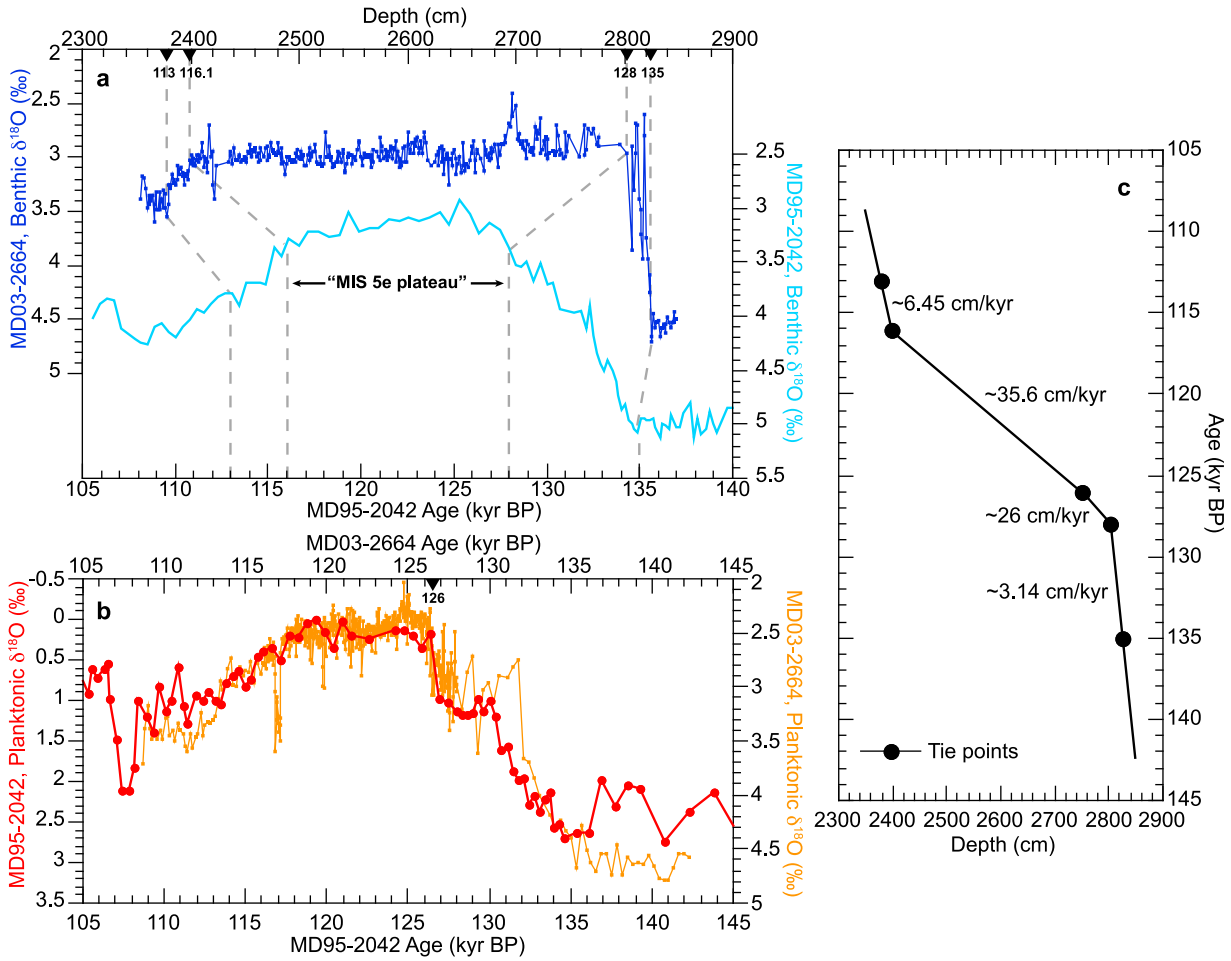

Figure 3. (a) The MD03-2664 benthic δ^{18}O record plotted versus core depth, together with the MD95-2042 benthic δ^{18}O record [*Shackleton et al.*, 2000] plotted versus age (age model after *Shackleton et al.* [2002, 2003]). The dashed lines indicate the assigned age control point. (b) The MD03-2664 planktonic δ^{18}O record plotted using the benthic δ^{18}O derived age control points shown in Figure 3a together with the MD95-2042 planktonic δ^{18}O record. Another tie point (at 126 kyr BP) is assigned based on the similar abrupt planktonic shift observed in both records. (c) Depth (cm) versus age (kyr BP) plot for MD03-2664, showing tie points and sedimentation rates.

due to enhanced biogenic carbonate fluxes and increases in detrital supply due to GIS retreat at the onset of interglacial intervals [*Fagel and Hillaire-Marcel*, 2006; *Evans et al.*, 2007; *Hillaire-Marcel et al.*, 2011]. Collectively, these processes maintain high, but potentially also variable, interglacial sedimentation rates in the region.

4. Results

4.1. Late MIS 6 and Deglaciation

[14] At site MD03-2664, late MIS 6 is characterized by high δ^{18}O (~4.8‰) and very low δ^{13}C values (varying between −0.27‰ and 0.14‰) of *N. pachyderma* (s) (Figures 4d and 4e, respectively). The foraminiferal assemblages are dominated by the polar species *N. pachyderma* (s) (~98%) (Figure 5) and IRD fluctuations vary between 17% and 98% (Figure 4c). High *N. pachyderma* (s) abundances and δ^{18}O values prevail until the IRD layer at 2812–2820 cm (~130.8–133.4 kyr BP). During this interval, IRD% increases to 98–99.5%, marking an episode of massive iceberg discharge, most likely associated with Heinrich Event 11 (H11). During the H11 event SSTs decrease (Figure 4a). SST reconstruction from Mg/Ca analysis shows a 2°C cooling at the mid-point of H11, whereas MAT SST indicate an even larger cooling of up to 5°C. The latter is highly variable during the H11 event due to high standard deviation of the H11 MAT SST estimates (2–2.5°C; Figure 2d), which can most likely be attributed to the high abundance of *N. pachyderma* (s) spanning H11. According to core top assemblages, the correspondence between *N. pachyderma* (s) abundances and surface temperature weakens when approaching 100%, and therefore may correspond to a wide range of temperatures [*Kohfeld et al.*, 1996; *Prell et al.*, 1999; *Oppo et al.*, 2006].

[15] Following H11, both MAT and Mg/Ca based SST reconstructions suggest a ~4°C warming at the end of the H11 event (Figure 4), coincident with a decrease in the abundance of the polar planktonic species *N. pachyderma* (s)

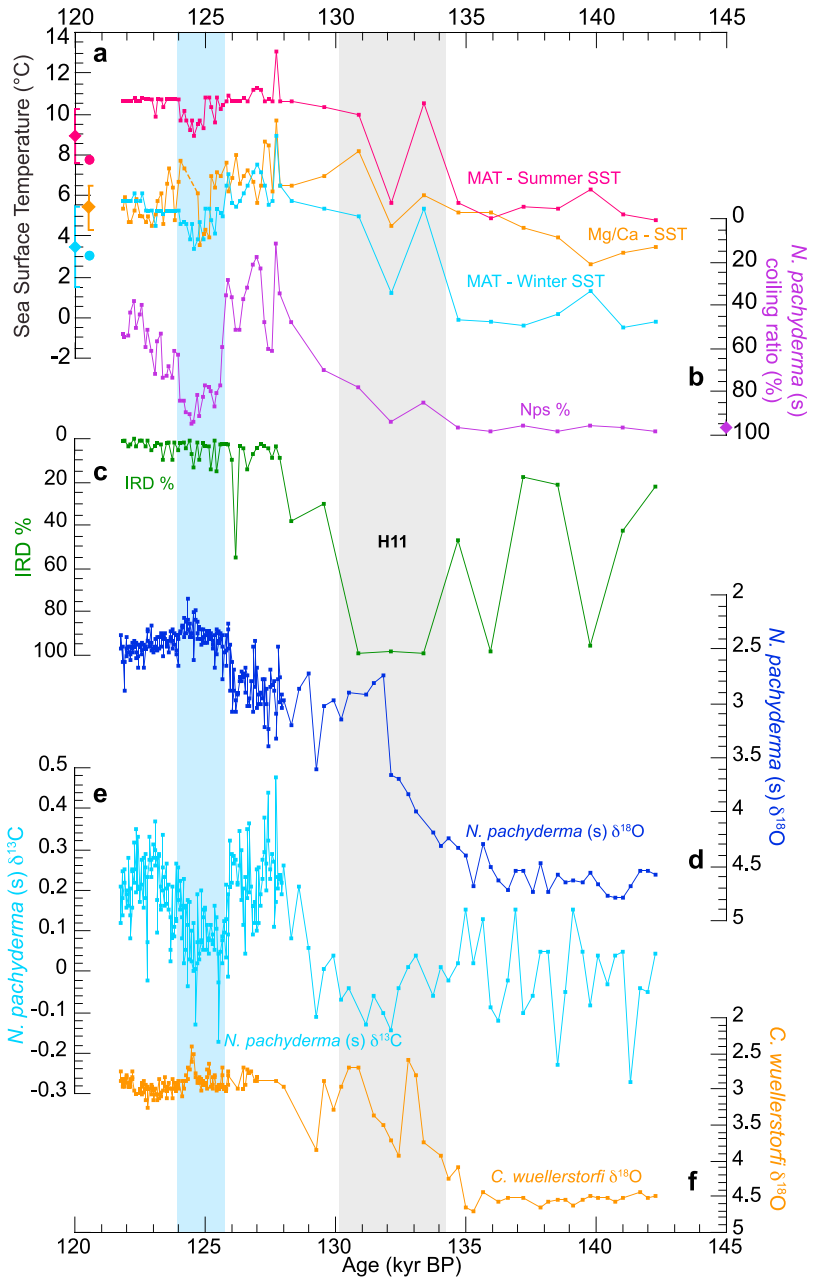

Figure 4. Proxy records from MD03-2664 plotted versus age (kyr BP). (a) SST estimates from MAT (summer (pink curve) and winter (light blue curve)) and Mg/Ca (orange curve) analysis, (b) *N. pachyderma* (s) coiling ratio (%) (purple curve), (c) IRD% (green curve), (d) planktonic (*N. pachyderma* (s) (dark blue curve)) δ^{18}O record, (e) planktonic (*N. pachyderma* (s) (light blue curve)) δ^{13}C record, and (f) benthic (*C. wuellerstorfi* (orange curve)) δ^{18}O record. The blue shaded interval indicates the cooling event, whereas H11 is marked by gray shading. Diamonds and circles in Figure 4a indicate the averaged SST in two core top samples from a nearby multicore and modern observations, respectively. Pink and blue diamonds show MAT summer (8.93 ± 1.35°C) and winter SSTs (3.44 ± 1.95°C), and the orange diamond shows Mg/Ca SST estimates (5.4 ± 1.1°C) from GS06-144-03MC A [*Kleiven et al.*, 2010]. Pink and blue circles indicate the modern SSTs (respectively 7.79°C for summer and 3.09°C for winter) near the core site (at 57°50′N, 48°50′W), obtained from the World Ocean Atlas 2009 [*Locarnini et al.*, 2010]. The purple diamond in Figure 4b indicates the average *N. pachyderma* (s) coiling ratio (%) from the two core top samples from GS06-144-03MC A [*Kleiven et al.*, 2010].

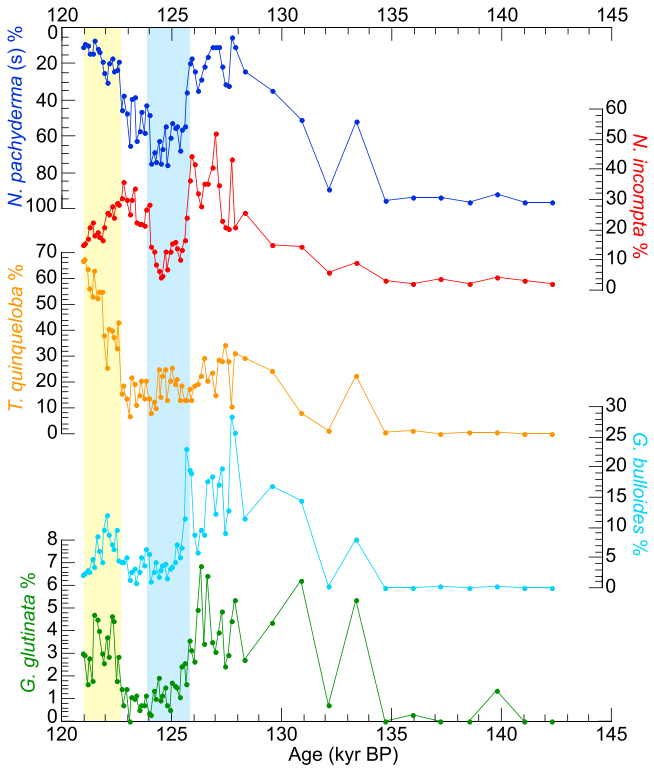

Figure 5. Relative abundances (%) of the most dominant planktonic species in core MD03-2664 plotted versus age (kyr BP). The blue band indicates the 126 kyr cooling event. The yellow band indicates the increase in *T. quinqueloba* relative abundance (%) indicating enhanced influx of Atlantic waters/Irminger Current (IC) off southern Greenland after ~122.5 kyr BP.

and increases in the abundances of subpolar-transitional species such as *N. incompta*, *T. quinqueloba*, *G. bulloides* and *G. glutinata* (Figure 5). This MIS 6/5e transition is also marked by a ~1.5‰ glacial to interglacial decrease in $\delta^{18}O$ of *N. pachyderma* (s) at ~132.5 kyr BP. Following the end of H11, $\delta^{13}C$ values of *N. pachyderma* (s) also increase from −0.11‰ to 0.21‰.

4.2. MIS 5e

4.2.1. Peak Warmth (2804–2740 cm, ~128.5–126 kyr BP)

[16] SST estimates from MAT and Mg/Ca results indicate that the peak warmth conditions were reached early in MIS 5e, between ~128.5–126 kyr BP (Figure 4a). During this period, the foraminiferal assemblage is dominated by subpolar-transitional species *N. incompta, T. quinqueloba*, *G. bulloides* and *G. glutinata* (Figure 5). The relative abundance and coiling ratio of *N. incompta* reach maxima of 52% and 88% respectively at 2796 cm (~127.7 kyr BP), indicating that warm surface temperatures were reached early in MIS 5e. The foraminiferal assemblage in the 2736–2812 cm core interval (~125.5–130.8 kyr BP) also includes warm-water species such as *N. dutertrei*, *G. inflata*, *G. scitula*, *G. ruber* (w), *O. universa*, and *G. crassaformis* in minor amounts, which are known to adapt to transitional, subtropical and tropical waters [*Tolderlund and Bé*, 1971]. The abundance of these rare species does not exceed 1% of the total foraminiferal assemblage, except for the transitional species *G. inflata*, which reaches up to 4% at 2796 cm (~127.7 kyr BP). This period of warmth is also characterized by generally very low IRD content (<5%), except at 2756 cm (~126.2 kyr BP) when IRD abundances reach 54% (Figure 4).

[17] Despite the faunal and Mg/Ca evidence for warmth early in MIS 5e, $\delta^{18}O$ values of *N. pachyderma* (s) remain at intermediary values close to ~3‰ through the 132.5–126 kyr BP interval with two brief minima recorded at ~127.8 kyr BP and 126.9 kyr BP. This $\delta^{18}O$ plateau is followed by a large (~0.8‰) $\delta^{18}O$ decrease at ~126 kyr BP. This interval of relatively stable but intermediary (~3‰) planktonic $\delta^{18}O$ values—coeval with high SSTs—bears strong resemblance in structure to the shoulder found in *Shackleton et al.*'s [2003] MIS 5e planktonic $\delta^{18}O$ record off the Iberian Margin (Figure 3b).

4.2.2. MIS 5e Cooling Event (2740–2678 cm, ~126–124 kyr BP)

[18] Warm surface temperatures prevailed until the (planktonic) isotopic peak of MIS 5e, when it was interrupted by a transient cooling evident in all proxy records. This cooling event is associated with the $\delta^{18}O$ shift at 126 kyr BP (Figure 4). The abrupt ~0.8‰ decrease in the *N. pachyderma* (s) $\delta^{18}O$ record at ~126 kyr BP occurs over 4 cm, equivalent to ~120 years on our current age model—although sedimentation rates may vary between control

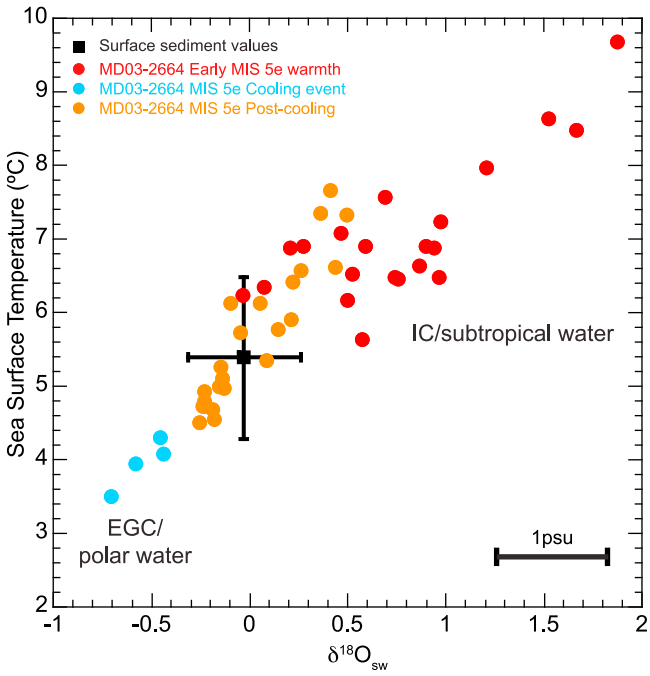

Figure 6. Mg/Ca based SST-$\delta^{18}O_{sw}$ estimates from MD03-2664 displayed on a crossplot. Red, light blue and orange circles mark early MIS 5e warmth, cooling and post-cooling intervals respectively. Black square indicates the Mg/Ca derived core top SST and $\delta^{18}O_{sw}$ value from a nearby multicore (GS06-144-03MC A [*Kleiven et al.*, 2010]), black lines show the error estimates.

points making precise estimates difficult. The coiling ratio of *N. pachyderma* shifts somewhat more gradually, over ~20 cm, from a 72% *N. incompta* abundance to 86% *N. pachyderma* (s). The total foraminiferal assemblage becomes dominated by the polar planktonic foraminifera *N. pachyderma* (s), indicating a strong shift toward 'polar-like' hydrographic conditions in the northern SPG at this time.

[19] Although shorter in duration, the Mg/Ca SST reconstruction also indicates cooling (Figure 4a). At 2724 cm (~125.2 kyr BP) SSTs decrease from ~7°C to ~4°C, reaching the coldest temperatures at 2708 cm (~124.8 kyr BP), similar to modern day values of EGC waters (e.g., potential temperature of polar origin waters of EGC is 3 ± 1.4°C in spring [*Holliday et al.*, 2006]). Likewise, SST estimates from MAT suggests a cooling of ~4°C during winter and 2°C during summer, attaining the coldest temperatures at 2700 cm. The high standard deviation of MAT SSTs (~1.6°C for summer and ~2.5°C for winter estimates, Figure 2d) during the cooling event is most likely due to the high *N. pachyderma* (s) abundances. Thus, assemblages and Mg/Ca SST estimates document similar magnitudes of cooling—both indicating SSTs dropped to near modern (oceanographic)/core top (late Holocene) values (Figure 4a). The shorter duration of the Mg/Ca event may be due to the three SST estimates that were rejected because of possible contamination (Figures 2 and 4).

[20] Other hydrographic changes are also observed during the ~126 kyr BP cooling event. The $\delta^{13}C$ of *N. pachyderma* (s) decreases by 0.3–0.5‰ during this period (Figure 4). The $\delta^{18}O$ values of *N. pachyderma* (s) also reach their MIS 5e minimum within this cooling, approaching 2.0‰ at 124.4 kyr BP—at nearly the same time as the coiling ratios of *N. pachyderma* (s) reach ~94%. Taken together, these results suggest that the 126-kyr transition represents a marked change in hydrographic conditions toward much more polar or EGC-like (colder, fresher, lower $\delta^{13}C$) water, at the core site.

[21] To further compare our results with modern data we compare SST and $\delta^{18}O_{sw}$ changes in order help to contextualize the scale and origin of these paleo-hydrographic changes. The $\delta^{18}O_{sw}$ (salinity) and SST records show close temporal covariance (Figure 6). Although the uncertainty on each individual salinity value is high (~1 psu) the linear T-$\delta^{18}O_{sw}$ slope suggests a simple (two end-members) control for the variance over time. The nature of this T-$\delta^{18}O_{sw}$ relationship, varying between warm/saline (high $\delta^{18}O_{sw}$) and cool/fresh (low $\delta^{18}O_{sw}$) conditions, is similar to that observed spatially in the North Atlantic today—supporting a role for shifting fresh (EGC) and saline (IC) influences at the core site. The saline and warm water during the early MIS 5e (~128–127 kyr BP) suggests not only a greater contribution of IC water to our site, but a stronger inflow of the warm, saline surface North Atlantic Current into this limb of the SPG. After 126 kyr BP $\delta^{18}O_{sw}$ values drop to ~−0.5‰, similar to values observed in the EGC today—consistent with increased EGC influence at this time. Although such estimates entail large uncertainties since paleo water mass $\delta^{18}O_{sw}$ end-members are not constrained, the large relative shift nevertheless suggests a marked change in the SPG and freshwater pathways/fluxes after 126 kyr BP (Figures 6 and 7).

4.2.3. Post-Cooling (2678–2600 cm, 124–121.7 kyr BP)

[22] The end of the cooling event is marked by a gradual influx of the subpolar-transitional species *N. incompta.* The abundance of *N. incompta* increases up to a maximum of 34%, but does not reach as high (52%) as during early MIS 5e warmth (Figure 5). Mg/Ca and MAT based SST estimates also support a return to warm conditions at the core site. Only the MAT summer estimates indicate that SSTs returned fully to pre-cooling event values, while MAT winter estimates and Mg/Ca results indicate slightly lower SSTs than the peak values observed in early MIS 5e (Figures 4a and 7e).

[23] Another hydrographic shift is recorded by the foraminiferal assemblage data during the post-cooling interval. A noticeable increase in the *T. quinqueloba* relative abundance is observed after the milder conditions gradually returned and stabilized (Figure 5). The relative abundance of *T. quinqueloba* increases in two steps, from 15% to 43% at 2630 cm (~122.6 kyr BP), and to 55% at 2602 cm (~121.8 kyr BP) (Figure 5). Today *T. quinqueloba* is found in polar to transitional regions [*Tolderlund and Bé*, 1971], and is used as an indicator of the Arctic front [e.g., *Fronval et al.*, 1998]. Therefore, the sharp increase in the *T. quinqueloba* percentage in core MD03-2664 after 122.5 kyr BP (together with the increase in other subpolar species' abundance, i.e., *G. bulloides*, *G. glutinata*) indicates an enhanced influx of Atlantic waters/Irminger Current (IC) off southern Greenland (i.e., a more proximal Arctic front).

[24] One possible caveat to this observation is that *T. quinqueloba*, census results have been found to vary with mesh size leading to different results and interpretations [e.g., *Kandiano and Bauch*, 2002]. However, other studies observed almost no difference [e.g., *Johannessen et al.*, 1994]. Records from southwest of Iceland and eastern subpolar North Atlantic show increases in the *T. quinqueloba* abundance coeval with those observed at our site—peaking near the MIS 5e/5d transition [*Oppo et al.*, 1997, 2001, 2007]. Similarly, *Fronval et al.* [1998] observed increasing *T. quinqueloba* percentage at a core location in the Iceland Sea at this time, indicating that the Arctic Front reached its most westerly position in the Nordic Seas at ~120–118 kyr BP. Increased influence of Atlantic waters in the southern Iceland Sea may reflect a relatively stronger IC, or alternatively reduced influence of polar waters from the EGC [*Fronval et al.*, 1998].

5. Discussion

[25] Our new high-resolution multiproxy record from the Eirik Drift provides insights into the nature and timing of subpolar North Atlantic hydrography and climatic variability during the last interglacial period. Our results indicate that during MIS 5e, North Atlantic surface ocean hydrography and climate experienced a number of distinct states including warmer than present conditions early in the last interglacial period.

5.1. Early MIS 5e Warmth

[26] Today, the left-coiling (sinistral) form of *N. pachyderma* is the dominant species in polar regions, whereas the right-coiling (dextral) form is found in warmer regions. *N. pachyderma* (s) is found in water temperatures between

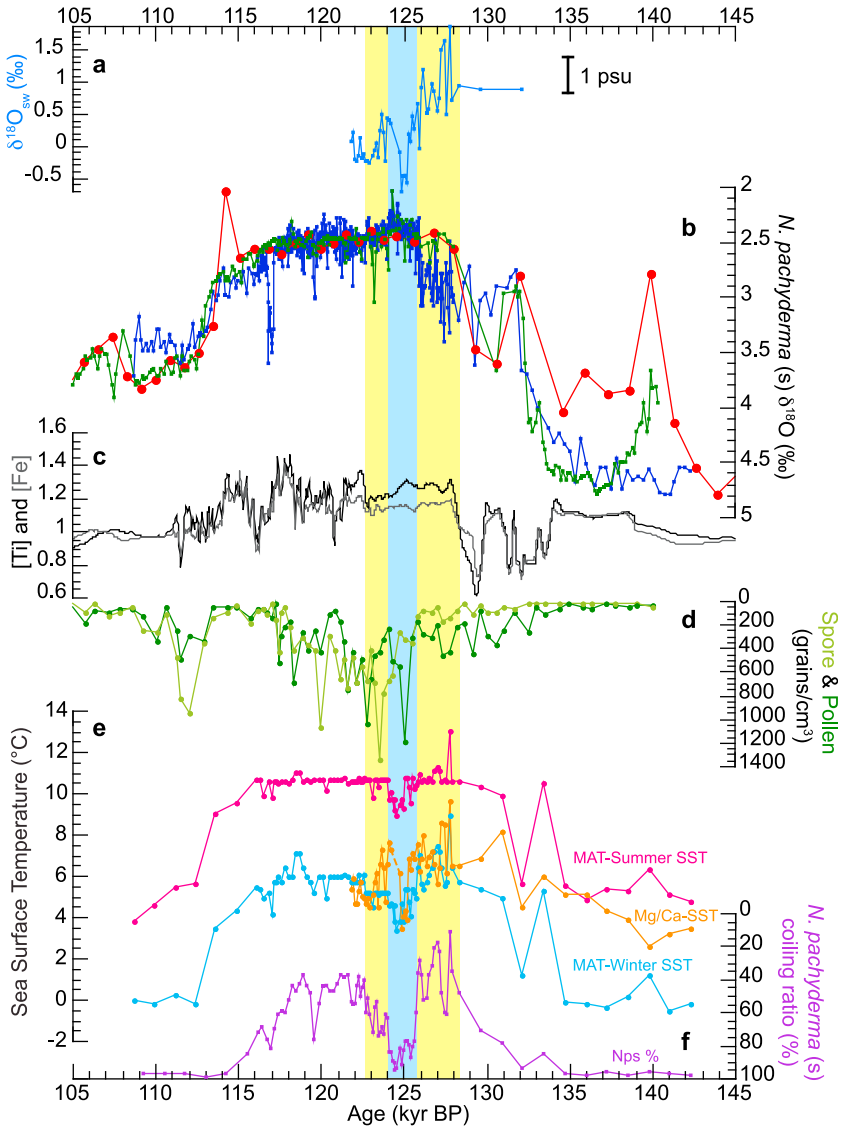

Figure 7. (a) The $\delta^{18}O_{sw}$ estimates for the MIS 5e plateau derived from paired Mg/Ca and $\delta^{18}O$ measurements of *N. pachyderma* (s) from Core MD03-2664 (blue curve); (b) the *N. pachyderma* (s) $\delta^{18}O$ records of MD03-2664 (dark blue curve), HU90-013-013 (green curve) [*Hillaire-Marcel et al.*, 1994] and MD99-2227 (red curve) [*Carlson et al.*, 2008]; (c) [Ti] and [Fe] records of MD99-2227 [*Carlson et al.*, 2008] (black and gray curves, respectively); (d) spore and pollen concentrations of HU90-013-013 (light and dark green curves, respectively) [*de Vernal and Hillaire-Marcel*, 2008]; (e) SST estimates from MAT (summer (pink curve) and winter (light blue curve)) and Mg/Ca (orange curve) analysis; and (f) *N. pachyderma* (s) coiling ratio (%) (purple curve). To facilitate the inter-site comparison, cores are plotted on the MD03-2664 age model by matching oxygen isotope records between the sites (Figure 7b). MAT SST estimates and *N. pachyderma* (s) coiling ratio (%) are plotted on 8 cm resolution for the 2350–2600 cm interval and on 4 cm for the 2600–2850 cm interval. The *N. pachyderma* (s) $\delta^{18}O$ record and spore and pollen concentrations of HU90-013-013 were obtained from the GEOTOP Paleoceanographic database at http://www.geotop.ca/index.php. The yellow band indicates the interval for the major GIS melting based on *Carlson et al.* [2008], and the blue band indicates the cooling event recorded at site MD03-2664.

−1°C and 8°C, reaches highest concentrations below 2°C, and rapidly decreases in waters warmer than 5°C [*Tolderlund and Bé*, 1971]. Large shifts (between 0% and 100%) in core top and modern percentage abundances of *N. pachyderma* (s) indicate approximately an 8°C SST change [*Kohfeld et al.*, 1996]. In the *N. pachyderma* (s) dominated polar regions, typical coiling ratios of *N. incompta* (*N. pachyderma* (dex)) are between 1% and 5 ± 1% from counts of 300 individuals [*Bauch et al.*, 2003]. The *N. pachyderma* (s) percentage of total planktonic foraminifera in modern pelagic sediments off southern Greenland, near the location of Core MD03-2664 from the

Eirik Drift, is above 95% [*Pflaumann et al.*, 2003]. Modern foraminiferal assemblages in the top two samples of a multicore taken adjacent to MD03-2664 (GS06-144-03MC A 57°28.71′N, 48°36.93′W, 3432 m water depth [*Kleiven et al.*, 2010]) have an average *N. pachyderma* (s) coiling ratio of 97% (Figure 4b).

[27] In contrast to the dominance of polar foraminifera in modern assemblages, the abundance of *N. incompta* was dominant through the early MIS 5e, between ~128.5 and ~126 kyr BP in MD03-2664. During this interval the abundance of transitional-subpolar species such as *T. quinqueloba*, *G. bulloides* and *G. glutinata* also increased, and even subtropical-tropical species were present in minor amounts. The high relative abundance of *N. incompta*, reaching a maximum of 52%, together with the relatively warmer-water fauna observed at this interval, depicts a period when surface water conditions off of southern Greenland supported a distinctly warmer planktonic fauna than presently.

[28] A warmer-than-today early MIS 5e is also supported by SST estimates reconstructed from MAT and Mg/Ca analysis. During early MIS 5e, both records reach peak warmth conditions at 2796 cm (~127.7 kyr BP). MAT summer SSTs rose to ~11 ± 1.33°C (peak 13°C), and MAT winter SSTs rose to ~7°C (peak 9°C) (Figure 4). Modern ocean temperatures (57°50′N, 48°50′W) are 3.09°C in winter (January–March) and 7.79°C in summer (July–September) [*Locarnini et al.*, 2010]—close to the core top MAT SST estimates of ~3 ± 1.9°C and ~9 ± 1.4°C for winter and summer [*Kleiven et al.*, 2010], respectively (Figure 4a). Hence, both modern and core top MAT SSTs indicate ~3–5°C colder modern conditions at the core site than during early MIS 5e.

[29] Mg/Ca-SST estimates of 7–10°C during early MIS 5e fall between the values from MAT summer and winter estimates (Figure 4a), suggesting they may be recording spring conditions, consistent with the spring bloom of *N. pachyderma* (s) [e.g., *Tolderlund and Bé*, 1971; *Jonkers et al.*, 2010]. Likewise, modern core top Mg/Ca-SST values of 5.4 ± 1.1°C fall squarely between winter (3.09°C) and summer (7.79°C) ocean temperatures in this region [*Locarnini et al.*, 2010]. Thus Mg/Ca results also suggest that peak early MIS 5e SSTs (7–10°C) were ~2–5°C warmer than modern (core top = 5.4 ± 1.1°C) (Figure 4a).

[30] The warm surface temperatures prevailed until ~126 kyr BP when they were terminated by a cooling event. This transition occurred over a few centuries and the cool period that followed prevailed for ~1600 years (spanning ~54 cm of core) until milder conditions gradually returned. Hydrographic changes associated with the cooling, such as a marked freshening (low $\delta^{18}O_{sw}$) and decrease in planktonic $\delta^{13}C$, suggest a period of markedly different hydrography south of Greenland following the ~126 kyr BP transition.

5.2. Origin of Hydrographic Changes

[31] What could cause cooling and freshening at this site when the high latitude Northern Hemisphere summer insolation was near its peak? Given our core location, rapid melting of the GIS and shifts in surface ocean currents (water masses) relative to the core site are obvious candidates. The inferred freshening ($\delta^{18}O_{sw}$ decrease) associated with the cold event may provide important constraints on the mechanisms at play. The fresh and cold EGC, which lies just north of the core site today, is a likely candidate for transporting cool/fresh water to the core site. Other sources of freshwater include precipitation, river runoff, meltwater from sea ice, inflows from the Pacific Ocean, and meltwater from continental ice, i.e., the GIS; which affect the fresh water flux along the EGC pathway [*Aagaard and Carmack*, 1989]. *Sutherland and Pickart* [2008] computed the freshwater budget of the EGC and the East Greenland Coastal Current (EGCC)—which is the inner branch of the EGC—system and found that the largest contribution came from sea ice, advected from the Arctic Ocean through Fram Strait and Denmark Strait, melting en-route to Cape Farewell during summer. In addition, glacial meltwater from the GIS is an important source of fresh water to the northern North Atlantic and the EGC system and could influence hydrography at the core site—amplifying/dampening any dynamic "circulation" related changes.

[32] The possibility for GIS influence bears further consideration since studies show that during the last interglacial period sea level was most likely up to 6.6 m higher than present [*Kopp et al.*, 2009], and GIS melting contributed 1.9–5.5 m of this higher sea level with the southern GIS shrinking [*Cuffey and Marshall*, 2000; *Otto-Bliesner et al.*, 2006; *Colville et al.*, 2011]. *Carlson et al.* [2008] studied the response of the GIS during the last two deglaciations using [Ti] and [Fe] in sediments from a nearby core, MD99-2227, on the Eirik Drift (Figure 1) to reconstruct summer melting. They proposed that the major ice margin retreat began following the MIS 6/5e transition with high and steady runoff in the 128–122.5 kyr BP interval concluding that the southern GIS response was synchronous with deglacial North Atlantic warming and potentially correlated with the interglacial atmospheric CH_4 peak at ~127 kyr BP [*Spahni et al.*, 2005]. Comparing the [Ti] and [Fe] records of *Carlson et al.* [2008] with our results (Figure 7), shows that the cool and fresh (low $\delta^{18}O_{sw}$) event recorded between ~126–124 kyr BP at site MD03-2664, does indeed coincide with the highest rates of GIS melting (Figure 7)—consistent with a role of ice sheet melting during this period. A recent paper by *Colville et al.* [2011] further supports rapid GIS melting in this interval. Based on Sr-Nd-Pb isotope ratios of sediments from the Eirik Drift core MD99-2227, they suggest continuous melting of GIS throughout the last interglacial period with the greatest southern GIS retreat occurring between ~127 and 120 kyr BP [*Colville et al.*, 2011].

[33] Pollen and spore concentrations of MIS 5e provide additional clues to GIS activity during the cooling event. The pollen record from Core HU90-013-013, also retrieved from the Eirik Drift (Figure 1), has been used as a proxy for the extent of the GIS since it provides information on the pollen production and vegetation density of southern Greenland [*de Vernal and Hillaire-Marcel*, 2008]. The detailed paleobotany studies of MIS 5e from Core HU90-013-013 document a rapid development of shrub tundra and dense fern vegetation over southern Greenland following ice retreat during early MIS 5e [*de Vernal and Hillaire-Marcel*, 2008]. Comparison of the spore and pollen concentrations of HU90-013-013 [*de Vernal and Hillaire-Marcel*, 2008] with the SST records of MD03-2664 shows that the cooling and freshening south of Greenland occurred during a period of

rapid expansion of vegetation in southern Greenland (Figure 7). The peak pollen concentration during this interval indicates mild conditions and increased vegetation and reduced Greenland ice volume; consistent with increased influence of meltwater (low $\delta^{18}O_{sw}$) from the retreating ice sheet. Low IRD concentrations at our site suggest that melting was taking place inland and not through coastal calving.

[34] However, GIS wasting alone cannot explain all of the observed hydrographic changes, including the anomalous warmth prior to 126 kyr BP, a time when GIS was also melting. For example, elevated [Ti] and [Fe] (high meltwater runoff) also corresponded to the peak warm conditions at site MD03-2664. This suggests that the GIS was decaying rapidly (and atmospheric CH_4 spiked [e.g., *Spahni et al.*, 2005]) during the period of early MIS 5e warmth in the northern rim of the SPG.

[35] Since elevated GIS melting occurs prior to the cooling and freshening starting at 126 kyr BP, and cannot explain the persistence of warm/saline conditions at our site prior to 126 kyr BP, we explore alternative mechanisms for these changes. One possible explanation for the post 126 kyr cooling and freshening is that circulation switched, with more IC (warm/salty) influence prior to 126 kyr giving way to more EGC (cold/fresh) influence after this time. The EGC provides an important dynamical link between the Arctic Ocean and North Atlantic and constitutes the main freshwater sink of the Arctic Ocean [*Schlichtholz and Houssais*, 1999]. On interdecadal timescales EGC freshwater fluxes play an important role in North Atlantic salinity changes [*Curry et al.*, 2003; *Curry and Mauritzen*, 2005] such as those observed during the Great Salinity Anomaly (GSA) that freshened the SPG [*Dickson et al.*, 1988]. Today, approximately one third of the EGC retroflects into the central Irminger basin, forming a pathway for freshwater into the interior of the SPG [*Holliday et al.*, 2007]. The drop in SSTs down to 2–3°C together with low $\delta^{18}O_{sw}$ is consistent with a much greater influence of EGC water at the core site. Indeed, the reconstructed $\delta^{18}O_{sw}$ values of −0.44 to −0.71‰ during the cooling (Figures 6 and 7) are similar to those found in the EGC today [*Schmidt et al.*, 1999].

[36] The surface water chemical changes observed in our core are also consistent with variations between EGC and IC influences at the core site. Regionally, the $\delta^{13}C$ values of *N. pachyderma* (s) show distinctly different values related to the different surface water masses in which they grow. Today, high $\delta^{13}C$ values correspond to cold Arctic waters, whereas low foraminiferal $\delta^{13}C$ is associated with perennially ice covered polar surface waters [*Johannessen et al.*, 1994]. The low $\delta^{13}C$ values observed during MIS 6 [*Fronval and Jansen*, 1997] and similarly during the last glacial maximum [*Sarnthein et al.*, 1995] reflected the dominance of extensive sea ice and polar surface waters. During the post 126 kyr BP cooling, foraminiferal $\delta^{13}C$ values drop close to values observed during MIS 6, consistent with increased polar (EGC) water influence at the core site.

5.3. SPG Dynamics

[37] We propose that early MIS 5e hydrographic shifts at the Eirik Drift are related to changes in SPG circulation. Past variability in the SPG circulation, including fast adjustments between strong and weak states of SPG, have been confirmed by modern and paleo-observations, and simulated in models [e.g., *Häkkinen and Rhines*, 2004; *Hátún et al.*, 2005; *Levermann and Born*, 2007; *Thornalley et al.*, 2009; *Born and Levermann*, 2010; *Born et al.*, 2010a, 2010b, 2011]. Surface wind stress [e.g., *Curry et al.*, 1998; *Böning et al.*, 2006], and density structure [*Eden and Willebrand*, 2001; *Häkkinen and Rhines*, 2004; *Hátún et al.*, 2005; *Levermann and Born*, 2007; *Häkkinen et al.*, 2008; *Lohmann et al.*, 2009; *Born et al.*, 2010a] both influence SPG circulation over recent decades and are likely candidates for modulating the SPG in the more distant past. These same processes are likely candidates for driving the type of MIS 5e property and faunal variations, between more IC like (warm/salty) and subpolar/EGC like (cold/fresh), reconstructed at our core site.

[38] The coincidence between subpolar North Atlantic warmth and peak atmospheric methane concentrations early in MIS 5e [*Spahni et al.*, 2005] would, if correct (age uncertainty), suggest a role for much broader atmospheric and hydrologic changes at this time. Past variations in methane concentrations are thought to be driven by changes in tropical climate and precipitation patterns [*Brook et al.*, 1999] which, in turn, were coupled to North Atlantic climate and sea ice changes—with North Atlantic warming associated with increased methane [*Brook et al.*, 1999; *Chiang et al.*, 2003, 2008]. Given these teleconnections, anomalous SPG warmth in early MIS 5e may help explain the origin of (or is at least consistent with) peaking atmospheric [CH_4] at this time and suggests that the local circulation changes could have been part of a much larger scale pattern involving high-low latitude atmospheric shifts.

[39] The occurrence of a hydrographic switch following the ramp up of GIS melting raises the possibility that freshwater flux (e.g., buoyancy) changes could also have been an important mechanism for altering SPG circulation. Modeling studies of MIS 5e climate and ocean circulation suggest a sensitivity of the SPG to freshening [*Born et al.*, 2010a], while modern observations show that freshwater fluctuations in the EGC system could impact both the SPG and the THC [*Cox et al.*, 2010]. SPG strength varies in relationship to the density difference between its center and rim [*Häkkinen and Rhines*, 2004; *Born et al.*, 2010a] and, at least in models, even relatively small fluctuations can trigger transitions between SPG states [*Levermann and Born*, 2007]. Enhanced freshwater flux into the SPG through the EGC causes cooling and freshening in the SPG region, which reduces the density gradient between the center and the rim of the gyre and weakens the SPG circulation [*Born et al.*, 2010a, 2011]. The weaker SPG circulation and weakening of the IC, carrying warm and saline tropical waters westward into the study area, act as positive feedbacks driving further cooling and freshening in the region [*Born et al.*, 2010a, 2011]. Therefore, during the warmer-than-present climatic conditions of early MIS 5e, a continuous freshwater flux could have been a trigger for switching the SPG into a weaker circulation. The fact that this transition occurs during a period of rapid GIS retreat points toward, or is at least consistent with, a role of GIS melting as an important source for the freshwater trigger.

[40] Regardless of how SPG changes were triggered (by wind stress and buoyancy changes), our records add to a growing body of evidence suggesting that early MIS 5e was a period of synoptic scale hydrographic reorganizations in the North Atlantic. For example, early MIS 5e transitions are also evident in records ranging from the subtropics to the Nordic Seas. For example, *Shackleton et al.* [2003] linked a planktonic $\delta^{18}O$ transition at ~126 kyr BP in a core off Portugal to the initiation of the Eemian and full terrestrial interglacial climate conditions over SW Europe. In addition, significant amounts of IRD and various SST proxies [*Bauch et al.*, 2011; *Van Nieuwenhove et al.*, 2011] indicate that the Nordic Seas were cool early in MIS 5e while the eastern North Atlantic was warm. This resulted in a steep temperature gradient across the Greenland-Scotland Ridge (GSR) suggesting a more east-west orientation of the Polar Front aligned with the GSR [*Rasmussen et al.*, 2003]. Given that SPG extent and circulation is important for communicating signals and changes between the North Atlantic and Nordic Seas [*Hátún et al.*, 2005], a switch in SPG circulation may help explain the spatial heterogeneity of climate evolution during early MIS 5e. For example, a weakened and contracted SPG after ~126 kyr BP would have exerted less influence in the eastern Atlantic and allowed warmer subtropical water to enter the Nordic Seas [after the mechanism of *Hátún et al.*, 2005]—warming the eastern Nordic Seas while cooling the Eirik Drift.

[41] Meltwater induced cooling is another mechanism that has been proposed for driving spatial heterogeneity in North Atlantic climate during MIS 5e [e.g., *Otto-Bliesner et al.*, 2006; *Govin et al.*, 2012]. *Govin et al.* [2012] propose that the delayed establishment of peak interglacial conditions in the North Atlantic, Labrador and Norwegian Seas could be driven by meltwater induced cooling early in MIS 5e as ice sheets wasted away. However, their model results suggest that in many regions, including the northwestern SPG and Eirik Drift, this cooling only partially offsets the effects of higher insolation. Hence the early MIS 5e warmth evident in our records is consistent with their simulations and does not rule out an important role for freshwater mediation of early MIS 5e climate. Nevertheless, we suggest that the full range of surface water property changes evident in our early MIS 5e multiproxy records such as increased planktonic $\delta^{13}C$ and $\delta^{18}O_{sw}$ (salinity) are not expected as a direct response to local insolation and meltwater increases—suggesting changes in regional (SPG) circulation still played a role in modulating the influence of EGC and IC in our study area.

6. Summary and Conclusions

[42] New high-resolution multiproxy records document late MIS 6 and early MIS 5e variability in climate and surface ocean hydrography off southern Greenland. SSTs peaked at levels ~3–5°C warmer than today early in MIS 5e and remained anomalously warm for ~2500 years. These anomalously warm surface temperatures were interrupted by a cooling starting at ~126 kyr BP. This cooling event, recorded in SST estimates and foraminiferal assemblages, is also marked by an abrupt shift to lower planktonic (*N. pachyderma* (s)) $\delta^{18}O$ values that persist through the rest of MIS 5e. A similar planktonic $\delta^{18}O$ trend is also documented in the eastern subtropical North Atlantic [*Shackleton et al.*, 2003], and in the Nordic Seas [*Bauch et al.*, 2011]. Following the cooling event, SSTs gradually increased near to early MIS 5e levels. During this post-cooling interval, at ~122.5 kyr BP, the relative abundance of *T. quinqueloba* increased sharply and dominated the foraminiferal assemblage. This indicates an enhanced influence of Atlantic waters/IC off southern Greenland and an increase in the fraction of relatively warm and saline subtropical waters.

[43] Taken together our results suggest that the hydrography and circulation of the North Atlantic SPG had multiple interglacial states or modes and that relatively rapid switches between these modes occurred. The changes involved shifts in freshwater fluxes/distributions, most likely related to changes in SPG circulation, swaying the balance between EGC and IC influences at the study area. Similar shifts in SPG properties have been linked to changes in NAO over recent decades [*Bersch*, 2002; *Flatau et al.*, 2003; *Häkkinen et al.*, 2008] suggesting a role for atmospheric forcing. The coincidence of the largest hydrographic switch at ~126 kyr BP with dramatic freshening of surface waters and rapid GIS retreat also raises the possibility that freshwater from GIS melting may have amplified, or even triggered, the type of slowdown in SPG circulation (and extent) seen in models forced with freshwater [e.g., *Levermann and Born*, 2007; *Born et al.*, 2010a].

[44] On a broader scale, mode switches in North Atlantic and SPG circulation may provide a dynamical mechanism for reconciling some of the spatiotemporal heterogeneities documented during MIS 5e (and Eemian) marine and terrestrial records of the North Atlantic. Given that the switches between circulation modes occurred rapidly, and during a period of warmer-than-present conditions and GIS melting, further characterization and modeling of these states and their activation thresholds may be highly relevant for understanding and predicting regional climate evolution in our future.

[45] **Acknowledgments.** The authors are grateful to IPEV, the captain and the crew of the *Marion Dufresne*, and the co-chief and scientific party of the IMAGES P.I.C.A.S.S.O cruise. We acknowledge J. Wright, who did a preliminary isotope study allowing us to locate stage 5e in the core, and thank A. Carlson for providing [Ti] and [Fe] records of MD99-2227. O. H. Otterå and A. Born are thanked for useful discussions, and comments from two anonymous reviewers helped us improve the manuscript. This work is a contribution of the European Science Foundation EuroMARC program, through the AMOCINT project, funded through grants from the Research Council of Norway (RCN) and contributes to EU-FP7 IP Past4Future. N. Irvalı was additionally funded by an ESF EUROCORES Short-term Visit grant and a RCN Leiv Eiriksson mobility grant to support research stays at the University of Edinburgh, UK, and Woods Hole Oceanographic Institution, USA, respectively, during which parts of the data for this paper were acquired. U. Ninnemann was funded by a University of Bergen Meltzer research grant. This is publication A387 from the Bjerknes Centre for Climate Research.

References

Aagaard, K., and E. C. Carmack (1989), The role of sea ice and other freshwater in the Arctic circulation, *J. Geophys. Res.*, *94*(C10), 14,485–14,498, doi:10.1029/JC094iC10p14485.

Antonov, J. I., D. Seidov, T. P. Boyer, R. A. Locarnini, A. V. Mishonov, and H. E. Garcia (2010), *World Ocean Atlas 2009*, vol. 2, *Salinity*, *NOAA Atlas NESDIS*, vol. 69, edited by S. Levitus, 184 pp., NOAA, Silver Spring, Md.

Bauch, H. A., and H. Erlenkeuser (2008), A "critical" climatic evaluation of last interglacial (MIS 5e) records from the Norwegian Sea, *Polar Res.*, *27*(2), 135–151, doi:10.1111/j.1751-8369.2008.00059.x.

Bauch, D., J. Carstens, and G. Wefer (1997), Oxygen isotope composition of living Neogloboquadrina pachyderma (sin.) in the Arctic Ocean, *Earth Planet. Sci. Lett.*, *146*(1–2), 47–58, doi:10.1016/S0012-821X(96)00211-7.

Bauch, D., K. Darling, J. Simstich, H. A. Bauch, H. Erlenkeuser, and D. Kroon (2003), Palaeoceanographic implications of genetic variation in living North Atlantic *Neogloboquadrina pachyderma*, *Nature*, *424*(6946), 299–302, doi:10.1038/nature01778.

Bauch, H. A., E. S. Kandiano, J. Helmke, N. Andersen, A. Rosell-Mele, and H. Erlenkeuser (2011), Climatic bisection of the last interglacial warm period in the Polar North Atlantic, *Quat. Sci. Rev.*, *30*(15–16), 1813–1818, doi:10.1016/j.quascirev.2011.05.012.

Bersch, M. (2002), North Atlantic Oscillation–induced changes of the upper layer circulation in the northern North Atlantic Ocean, *J. Geophys. Res.*, *107*(C10), 3156, doi:10.1029/2001JC000901.

Böning, C. W., M. Scheinert, J. Dengg, A. Biastoch, and A. Funk (2006), Decadal variability of subpolar gyre transport and its reverberation in the North Atlantic overturning, *Geophys. Res. Lett.*, *33*, L21S01, doi:10.1029/2006GL026906.

Born, A., and A. Levermann (2010), The 8.2 ka event: Abrupt transition of the subpolar gyre toward a modern North Atlantic circulation, *Geochem. Geophys. Geosyst.*, *11*(6), Q06011, doi:10.1029/2009GC003024.

Born, A., K. H. Nisancioglu, and P. Braconnot (2010a), Sea ice induced changes in ocean circulation during the Eemian, *Clim. Dyn.*, *35*(7–8), 1361–1371, doi:10.1007/s00382-009-0709-2.

Born, A., M. Kageyama, and K. H. Nisancioglu (2010b), Warm Nordic Seas delayed glacial inception in Scandinavia, *Clim. Past*, *6*(6), 817–826, doi:10.5194/cp-6-817-2010.

Born, A., K. H. Nisancioglu, and B. Risebrobakken (2011), Late Eemian warming in the Nordic Seas as seen in proxy data and climate models, *Paleoceanography*, *26*, PA2207, doi:10.1029/2010PA002027.

Brook, E. J., S. Harder, J. Severinghaus, and M. Bender (1999), Atmospheric methane and millennial-scale climate change, in *Mechanisms of Global Climate Change at Millennial Timescales*, *Geophys. Monogr. Ser*, edited by P. U. Clark, R. S. Webb, and L. D. Keigwin, pp. 165–175, AGU, Washington, D.C., doi:10.1029/GM112p0165.

Carlson, A. E., J. S. Stoner, J. P. Donnelly, and C. Hillaire-Marcel (2008), Response of the southern Greenland Ice Sheet during the last two deglaciations, *Geology*, *36*(5), 359–362, doi:10.1130/G24519A.1.

Chiang, J. C. H., M. Biasutti, and D. S. Battisti (2003), Sensitivity of the Atlantic Intertropical Convergence Zone to Last Glacial Maximum boundary conditions, *Paleoceanography*, *18*(4), 1094, doi:10.1029/2003PA000916.

Chiang, J. C. H., W. Cheng, and C. M. Bitz (2008), Fast teleconnections to the tropical Atlantic sector from Atlantic thermohaline adjustment, *Geophys. Res. Lett.*, *35*, L07704, doi:10.1029/2008GL033292.

Chough, S. K., R. Hesse, and J. Müller (1987), The Northwest Atlantic Mid-Ocean Channel of the Labrador Sea. IV. Petrography and provenance of the sediments, *Can. J. Earth Sci.*, *24*(4), 731–740, doi:10.1139/e87-071.

Colville, E. J., A. E. Carlson, B. L. Beard, R. G. Hatfield, J. S. Stoner, A. V. Reyes, and D. J. Ullman (2011), Sr-Nd-Pb Isotope Evidence for Ice-Sheet Presence on Southern Greenland During the Last Interglacial, *Science*, *333*(6042), 620–623, doi:10.1126/science.1204673.

Cox, K. A., J. D. Stanford, A. J. McVicar, E. J. Rohling, K. J. Heywood, S. Bacon, M. Bolshaw, P. A. Dodd, S. De la Rosa, and D. Wilkinson (2010), Interannual variability of Arctic sea ice export into the East Greenland Current, *J. Geophys. Res.*, *115*, C12063, doi:10.1029/2010JC006227.

Cuffey, K. M., and S. J. Marshall (2000), Substantial contribution to sea-level rise during the last interglacial from the Greenland ice sheet, *Nature*, *404*(6778), 591–594, doi:10.1038/35007053.

Curry, R., and C. Mauritzen (2005), Dilution of the northern North Atlantic Ocean in recent decades, *Science*, *308*(5729), 1772–1774, doi:10.1126/science.1109477.

Curry, R., M. S. McCartney, and T. M. Joyce (1998), Oceanic transport of subpolar climate signals to mid-depth subtropical waters, *Nature*, *391*(6667), 575–577, doi:10.1038/35356.

Curry, R., B. Dickson, and I. Yashayaev (2003), A change in the freshwater balance of the Atlantic Ocean over the past four decades, *Nature*, *426*(6968), 826–829, doi:10.1038/nature02206.

Darling, K. F., M. Kucera, D. Kroon, and C. M. Wade (2006), A resolution for the coiling direction paradox in *Neogloboquadrina pachyderma*, *Paleoceanography*, *21*, PA2011, doi:10.1029/2005PA001189.

de Vernal, A., and C. Hillaire-Marcel (2008), Natural variability of Greenland climate, vegetation, and ice volume during the past million years, *Science*, *320*(5883), 1622–1625, doi:10.1126/science.1153929.

Dickson, R. R., J. Meincke, S.-A. Malmberg, and A. J. Lee (1988), The "great salinity anomaly" in the Northern North Atlantic 1968–1982, *Prog. Oceanogr.*, *20*(2), 103–151, doi:10.1016/0079-6611(88)90049-3.

Eden, C., and J. Willebrand (2001), Mechanism of interannual to decadal variability of the North Atlantic circulation, *J. Clim.*, *14*(10), 2266–2280, doi:10.1175/1520-0442(2001)014<2266:MOITDV>2.0.CO;2.

Evans, H. F., J. E. T. Channell, J. S. Stoner, C. Hillaire-Marcel, J. D. Wright, L. C. Neitzke, and G. S. Mountain (2007), Paleointensity-assisted chronostratigraphy of detrital layers on the Eirik Drift (North Atlantic) since marine isotope stage 11, *Geochem. Geophys. Geosyst.*, *8*, Q11007, doi:10.1029/2007GC001720.

Fagel, N., and C. Hillaire-Marcel (2006), Glacial/interglacial instabilities of the Western Boundary Under Current during the last 365 kyr from Sm/Nd ratios of the sedimentary clay-size fractions at ODP site 646(Labrador Sea), *Mar. Geol.*, *232*(1–2), 87–99, doi:10.1016/j.margeo.2006.08.006.

Flatau, M. K., L. Talley, and P. P. Niiler (2003), The North Atlantic Oscillation, surface current velocities, and SST changes in the subpolar North Atlantic, *J. Clim.*, *16*(14), 2355–2369, doi:10.1175/2787.1.

Fronval, T., and E. Jansen (1997), Eemian and Early Weichselian (140–60 ka) paleoceanography and paleoclimate in the Nordic Seas with comparisons to Holocene conditions, *Paleoceanography*, *12*(3), 443–462, doi:10.1029/97PA00322.

Fronval, T., E. Jansen, H. Haflidason, and J. P. Sejrup (1998), Variability in surface and deep water conditions in the Nordic seas during the last interglacial period, *Quat. Sci. Rev.*, *17*(9–10), 963–985, doi:10.1016/S0277-3791(98)00038-9.

Gouzy, A., B. Malaizé, C. Pujol, and K. Charlier (2004), Climatic "pause" during Termination II identified in shallow and intermediate waters off the Iberian margin, *Quat. Sci. Rev.*, *23*(14–15), 1523–1528, doi:10.1016/j.quascirev.2004.03.002.

Govin, A., et al. (2012), Persistent influence of ice sheet melting on high northern latitude climate during the early Last Interglacial, *Clim. Past*, *8*(2), 483–507, doi:10.5194/cp-8-483-2012.

Häkkinen, S., and P. B. Rhines (2004), Decline of subpolar North Atlantic circulation during the 1990s, *Science*, *304*(5670), 555–559, doi:10.1126/science.1094917.

Häkkinen, S., H. Hátún, and P. Rhines (2008), Satellite Evidence of Change in the Northern Gyre, in *Arctic–Subarctic Ocean Fluxes*, edited by R. R. Dickson, J. Meincke, and P. Rhines, pp. 551–567, Springer, Dordrecht, doi:10.1007/978-1-4020-6774-7_24.

Hátún, H., A. B. Sandø, H. Drange, B. Hansen, and H. Valdimarsson (2005), Influence of the Atlantic Subpolar Gyre on the thermohaline circulation, *Science*, *309*(5742), 1841–1844, doi:10.1126/science.1114777.

Hátún, H., M. R. Payne, G. Beaugrand, P. C. Reid, A. B. Sandø, H. Drange, B. Hansen, J. A. Jacobsen, and D. Bloch (2009), Large bio-geographical shifts in the north-eastern Atlantic Ocean: From the subpolar gyre, via plankton, to blue whiting and pilot whales, *Prog. Oceanogr.*, *80*(3–4), 149–162, doi:10.1016/j.pocean.2009.03.001.

Hesse, R., and S. K. Chough (1980), The Northwest Atlantic Mid-Ocean Channel of the Labrador Sea: II. Deposition of parallel laminated levee-muds from the viscous sublayer of low density turbidity currents, *Sedimentology*, *27*(6), 697–711, doi:10.1111/j.1365-3091.1980.tb01656.x.

Hillaire-Marcel, C., A. de Vernal, G. Bilodeau, and G. Wu (1994), Isotope stratigraphy, sedimentation rates, deep circulation, and carbonate events in the Labrador Sea during the last ~200 ka, *Can. J. Earth Sci.*, *31*(1), 63–89, doi:10.1139/e94-007.

Hillaire-Marcel, C., A. de Vernal, G. Bilodeau, and A. J. Weaver (2001), Absence of deep-water formation in the Labrador Sea during the last interglacial period, *Nature*, *410*(6832), 1073–1077, doi:10.1038/35074059.

Hillaire-Marcel, C., A. de Vernal, and J. McKay (2011), Foraminifer isotope study of the Pleistocene Labrador Sea, northwest North Atlantic (IODP Sites 1302/03 and 1305), with emphasis on paleoceanographical differences between its "inner" and "outer" basins, *Mar. Geol.*, *279*(1–4), 188–198, doi:10.1016/j.margeo.2010.11.001.

Hiscott, R. N., M. Cremer, and A. E. Aksu (1989), Evidence from sedimentary structures for processes of sediment transport and deposition during post-Miocene time at Sites 645, 646, and 647, Baffin Bay and the Labrador Sea, *Proc. Ocean Drill. Program, Sci. Results*, *105*, 53–63.

Holliday, N. P., J. J. Waniek, R. Davidson, D. Wilson, L. Brown, R. Sanders, R. T. Pollard, and J. T. Allen (2006), Large-scale physical controls on phytoplankton growth in the Irminger Sea Part I: Hydrographic zones, mixing and stratification, *J. Mar. Syst.*, *59*(3–4), 201–218, doi:10.1016/j.jmarsys.2005.10.004.

Holliday, N. P., A. Meyer, S. Bacon, S. G. Alderson, and B. de Cuevas (2007), Retroflection of part of the east Greenland current at Cape Farewell, *Geophys. Res. Lett.*, *34*, L07609, doi:10.1029/2006GL029085.

Hunter, S., D. Wilkinson, E. Louarn, I. Nick McCave, E. Rohling, D. A. V. Stow, and S. Bacon (2007), Deep western boundary current

dynamics and associated sedimentation on the Eirik Drift, Southern Greenland Margin, *Deep Sea Res., Part I*, *54*(12), 2036–2066, doi:10.1016/j.dsr.2007.09.007.

Hutson, W. H. (1980), The Agulhas Current during the Late Pleistocene: Analysis of Modern Faunal Analogs, *Science*, *207*(4426), 64–66, doi:10.1126/science.207.4426.64.

Johannessen, T., E. Jansen, A. Flatøy, and A. C. Ravelo (1994), The relationship between surface water masses, oceanographic fronts and paleoclimatic proxies in surface sediments of the Greenland, Iceland Norwegian Seas, in *Carbon Cycling in the Glacial Ocean: Constraints on the Ocean's Role in Global Change*, *NATO ASI Ser., Ser. I*, vol. 17, edited by R. Zahn et al., pp. 61–86, Springer, Berlin.

Jonkers, L., G.-J. A. Brummer, F. J. C. Peeters, H. M. van Aken, and M. F. De Jong (2010), Seasonal stratification, shell flux, and oxygen isotope dynamics of left-coiling *N. pachyderma* and *T. quinqueloba* in the western subpolar North Atlantic, *Paleoceanography*, *25*, PA2204, doi:10.1029/2009PA001849.

Kandiano, E. S., and H. A. Bauch (2002), Implications of planktic foraminiferal size fractions for the glacial-interglacial paleoceanography of the polar North Atlantic, *J. Foraminiferal Res.*, *32*(3), 245–251, doi:10.2113/32.3.245.

Kleiven, H. F., Y. Rosenthal, and U. S. Ninnemann (2010), Climate and North Atlantic Deep Water variability since 600 AD., paper presented at 10th International Conference on Paleoceanography, Scripps Int. of Oceanogr., Univ. of Calif., San Diego, La Jolla.

Kohfeld, K. E., R. G. Fairbanks, S. L. Smith, and I. D. Walsh (1996), *Neogloboquadrina pachyderma* (sinistral coiling) as paleoceanographic tracers in polar oceans: Evidence from Northeast Water Polynya plankton tows, sediment traps, and surface sediments, *Paleoceanography*, *11*(6), 679–699, doi:10.1029/96PA02617.

Kopp, R. E., F. J. Simons, J. X. Mitrovica, A. C. Maloof, and M. Oppenheimer (2009), Probabilistic assessment of sea level during the last interglacial stage, *Nature*, *462*(7275), 863–867, doi:10.1038/nature08686.

Kozdon, R., A. Eisenhauer, M. Weinelt, M. Y. Meland, and D. Nürnberg (2009), Reassessing Mg/Ca temperature calibrations of *Neogloboquadrina pachyderma* (sinistral) using paired $\delta^{44/40}$Ca and Mg/Ca measurements, *Geochem. Geophys. Geosyst.*, *10*, Q03005, doi:10.1029/2008GC002169.

LeGrande, A. N., and G. A. Schmidt (2006), Global gridded data set of the oxygen isotopic composition in seawater, *Geophys. Res. Lett.*, *33*, L12604, doi:10.1029/2006GL026011.

Levermann, A., and A. Born (2007), Bistability of the Atlantic subpolar gyre in a coarse-resolution climate model, *Geophys. Res. Lett.*, *34*, L24605, doi:10.1029/2007GL031732.

Locarnini, R. A., A. V. Mishonov, J. I. Antonov, T. P. Boyer, H. E. Garcia, O. K. Baranova, M. M. Zweng, and D. R. Johnson (2010), *World Ocean Atlas 2009*, vol. 1, *Temperature, NOAA Atlas NESDIS*, vol. 68, edited by S. Levitus, 184 pp., NOAA, Silver Spring, Md.

Lohmann, K., H. Drange, and M. Bentsen (2009), Response of the North Atlantic subpolar gyre to persistent North Atlantic oscillation like forcing, *Clim. Dyn.*, *32*(2–3), 273–285, doi:10.1007/s00382-008-0467-6.

Lototskaya, A., and G. M. Ganssen (1999), The structure of Termination II (penultimate deglaciation and Eemian) in the North Atlantic, *Quat. Sci. Rev.*, *18*(14), 1641–1654, doi:10.1016/S0277-3791(99)00011-6.

Meland, M. Y., E. Jansen, H. Elderfield, T. M. Dokken, A. Olsen, and R. G. J. Bellerby (2006), Mg/Ca ratios in the planktonic foraminifer *Neogloboquadrina pachyderma* (sinistral) in the northern North Atlantic/Nordic Seas, *Geochem. Geophys. Geosyst.*, *7*, Q06P14, doi:10.1029/2005GC001078.

Nürnberg, D. (1995), Magnesium in tests of *Neogloboquadrina pachyderma* sinistral from high northern and southern latitudes, *J. Foraminiferal Res.*, *25*(4), 350–368, doi:10.2113/gsjfr.25.4.350.

Nürnberg, D., A. Müller, and R. R. Schneider (2000), Paleo-sea surface temperature calculations in the equatorial east Atlantic from Mg/Ca ratios in planktic foraminifera: A comparison to sea surface temperature estimates from $U^{K'}_{37}$, oxygen isotopes, and foraminiferal transfer function, *Paleoceanography*, *15*(1), 124–134, doi:10.1029/1999PA000370.

Oppo, D. W., M. Horowitz, and S. J. Lehman (1997), Marine core evidence for reduced deep water production during Termination II followed by a relatively stable substage 5e (Eemian), *Paleoceanography*, *12*(1), 51–63, doi:10.1029/96PA03133.

Oppo, D. W., L. D. Keigwin, J. F. McManus, and J. L. Cullen (2001), Persistent suborbital climate variability in marine isotope stage 5 and Termination II, *Paleoceanography*, *16*(3), 280–292, doi:10.1029/2000PA000527.

Oppo, D. W., J. F. McManus, and J. L. Cullen (2006), Evolution and demise of the Last Interglacial warmth in the subpolar North Atlantic, *Quat. Sci. Rev.*, *25*(23–24), 3268–3277, doi:10.1016/j.quascirev.2006.07.006.

Oppo, D. W., J. F. McManus, and J. L. Cullen (2007), Subpolar North Atlantic ODP980 MIS5 Sediment Data, ftp://ftp.ncdc.noaa.gov/pub/data/paleo/contributions_by_author/oppo2006/oppo2006.txt, World Data Cent. for Paleoclimatology, Boulder, Colo.

Otto-Bliesner, B. L., S. J. Marsha, J. T. Overpeck, G. H. Miller, and A. X. Hu (2006), Simulating arctic climate warmth and icefield retreat in the last interglaciation, *Science*, *311*(5768), 1751–1753, doi:10.1126/science.1120808.

Overpeck, J. T., T. Webb, and I. C. Prentice (1985), Quantitative interpretation of fossil pollen spectra: Dissimilarity coefficients and the method of modern analogs, *Quat. Res.*, *23*(1), 87–108, doi:10.1016/0033-5894(85)90074-2.

Pflaumann, U., et al. (2003), Glacial North Atlantic: Sea-surface conditions reconstructed by GLAMAP 2000, *Paleoceanography*, *18*(3), 1065, doi:10.1029/2002PA000774.

Prell, W. L. (1985), The stability of low-latitude sea surface temperatures: An evaluation of the CLIMAP reconstruction with emphasis on the positive SST anomalies, *Rep. TR025*, 60 pp., U.S. Dep. of Energy, Washington, D. C.

Prell, W. L., A. Martin, J. Cullen, and M. Trend (1999), Brown University Foraminiferal Database, http://www.ncdc.noaa.gov/paleo/metadata/noaa-ocean-5908.html, World Data Cent. for Paleoclimatology, Boulder, Colo.

Rasmussen, T. L., E. Thomsen, A. Kuijpers, and S. Wastegård (2003), Late warming and early cooling of the sea surface in the Nordic seas during MIS 5e (Eemian Interglacial), *Quat. Sci. Rev.*, *22*(8–9), 809–821, doi:10.1016/S0277-3791(02)00254-8.

Rosenthal, Y., M. P. Field, and R. M. Sherrell (1999), Precise determination of element/calcium ratios in calcareous samples using sector field inductively coupled plasma mass spectrometry, *Anal. Chem.*, *71*(15), 3248–3253, doi:10.1021/ac981410x.

Rosenthal, Y., et al. (2004), Interlaboratory comparison study of Mg/Ca and Sr/Ca measurements in planktonic foraminifera for paleoceanographic research, *Geochem. Geophys. Geosyst.*, *5*, Q04D09, doi:10.1029/2003GC000650.

Rudels, B., E. Fahrbach, J. Meincke, G. Budéus, and P. Eriksson (2002), The East Greenland Current and its contribution to the Denmark Strait overflow, *ICES J. Mar. Sci.*, *59*(6), 1133–1154, doi:10.1006/jmsc.2002.1284.

Sánchez Goñi, M. F., F. Eynaud, J. L. Turon, and N. J. Shackleton (1999), High resolution palynological record off the Iberian margin: Direct land-sea correlation for the Last Interglacial complex, *Earth Planet. Sci. Lett.*, *171*(1), 123–137, doi:10.1016/S0012-821X(99)00141-7.

Sarnthein, M., and R. Tiedemann (1990), Younger Dryas-style cooling events at glacial terminations I-VI at ODP Site 658: Associated benthic δ^{13}C anomalies constrain meltwater hypothesis, *Paleoceanography*, *5*(6), 1041–1055, doi:10.1029/PA005i006p01041.

Sarnthein, M., et al. (1995), Variations in Atlantic surface ocean paleoceanography, 50°–80°N: A time-slice record of the last 30,000 years, *Paleoceanography*, *10*(6), 1063–1094, doi:10.1029/95PA01453.

Schlichtholz, P., and M.-N. Houssais (1999), An investigation of the dynamics of the East Greenland Current in Fram Strait based on a simple analytical model, *J. Phys. Oceanogr.*, *29*(9), 2240–2265, doi:10.1175/1520-0485(1999)029<2240:AIOTDO>2.0.CO;2.

Schmidt, G. A., G. R. Bigg, and E. J. Rohling (1999), Global Seawater Oxygen-18 Database-v1.21, http://data.giss.nasa.gov/o18data/, NASA Goddard Inst. of Space Sci., New York.

Shackleton, N. J. (1974), Attainment of isotopic equilibrium between ocean water and benthonic foraminifera genus *Uvigerina*: Isotopic changes in the ocean during the last glacial, *Colloq. Int. C. N. R. S.*, *219*, 203–209.

Shackleton, N. J., M. A. Hall, and E. Vincent (2000), Phase relationships between millennial-scale events 64,000–24,000 years ago, *Paleoceanography*, *15*(6), 565–569, doi:10.1029/2000PA000513.

Shackleton, N. J., M. Chapman, M. F. Sánchez Goñi, D. Pailler, and Y. Lancelot (2002), The classic Marine Isotope Substage 5e, *Quat. Res.*, *58*(1), 14–16, doi:10.1006/qres.2001.2312.

Shackleton, N. J., M. F. Sánchez Goñi, D. Pailler, and Y. Lancelot (2003), Marine Isotope Substage 5e and the Eemian Interglacial, *Global Planet. Change*, *36*(3), 151–155, doi:10.1016/S0921-8181(02)00181-9.

Simstich, J., M. Sarnthein, and H. Erlenkeuser (2003), Paired δ^{18}O signals of *Neogloboquadrina pachyderma* (s) and *Turborotalita quinqueloba* show thermal stratification structure in Nordic Seas, *Mar. Micropaleontol.*, *48*(1–2), 107–125, doi:10.1016/S0377-8398(02)00165-2.

Skinner, L. C., and N. J. Shackleton (2005), An Atlantic lead over Pacific deep-water change across Termination I: Implications for the application of the marine isotope stage stratigraphy, *Quat. Sci. Rev.*, *24*(5–6), 571–580, doi:10.1016/j.quascirev.2004.11.008.

Spahni, R., et al. (2005), Atmospheric methane and nitrous oxide of the late pleistocene from Antarctic ice cores, *Science*, *310*(5752), 1317–1321, doi:10.1126/science.1120132.

Stirling, C. H., T. M. Esat, K. Lambeck, and M. T. McCulloch (1998), Timing and duration of the Last Interglacial: Evidence for a restricted interval of widespread coral reef growth, *Earth Planet. Sci. Lett.*, *160*(3–4), 745–762, doi:10.1016/S0012-821X(98)00125-3.

Sutherland, D. A., and R. S. Pickart (2008), The East Greenland Coastal Current: Structure, variability, and forcing, *Prog. Oceanogr.*, *78*(1), 58–77, doi:10.1016/j.pocean.2007.09.006.

Thornalley, D. J. R., H. Elderfield, and I. N. McCave (2009), Holocene oscillations in temperature and salinity of the surface subpolar North Atlantic, *Nature*, *457*(7230), 711–714, doi:10.1038/nature07717.

Tolderlund, D. S., and A. W. H. Bé (1971), Seasonal distribution of planktonic foraminifera in the western North Atlantic, *Micropaleontology*, *17*(3), 297–329, doi:10.2307/1485143.

Van Nieuwenhove, N., H. A. Bauch, F. Eynaud, E. Kandiano, E. Cortijo, and J.-L. Turon (2011), Evidence for delayed poleward expansion of North Atlantic surface waters during the last interglacial (MIS 5e), *Quat. Sci. Rev.*, *30*(7–8), 934–946, doi:10.1016/j.quascirev.2011.01.013.